LBNL-41854

ERNEST ORLANDO LAWRENCE BERKELEY NATIONAL LABORATORY

Effect of Uniaxial Stress on Gallium, Beryllium, and Copper-doped Germanium Hole Population Inversion Lasers

Danielle R. Chamberlin

Materials Sciences Division

Center for Advanced Materials

May 1998

M.S. Thesis

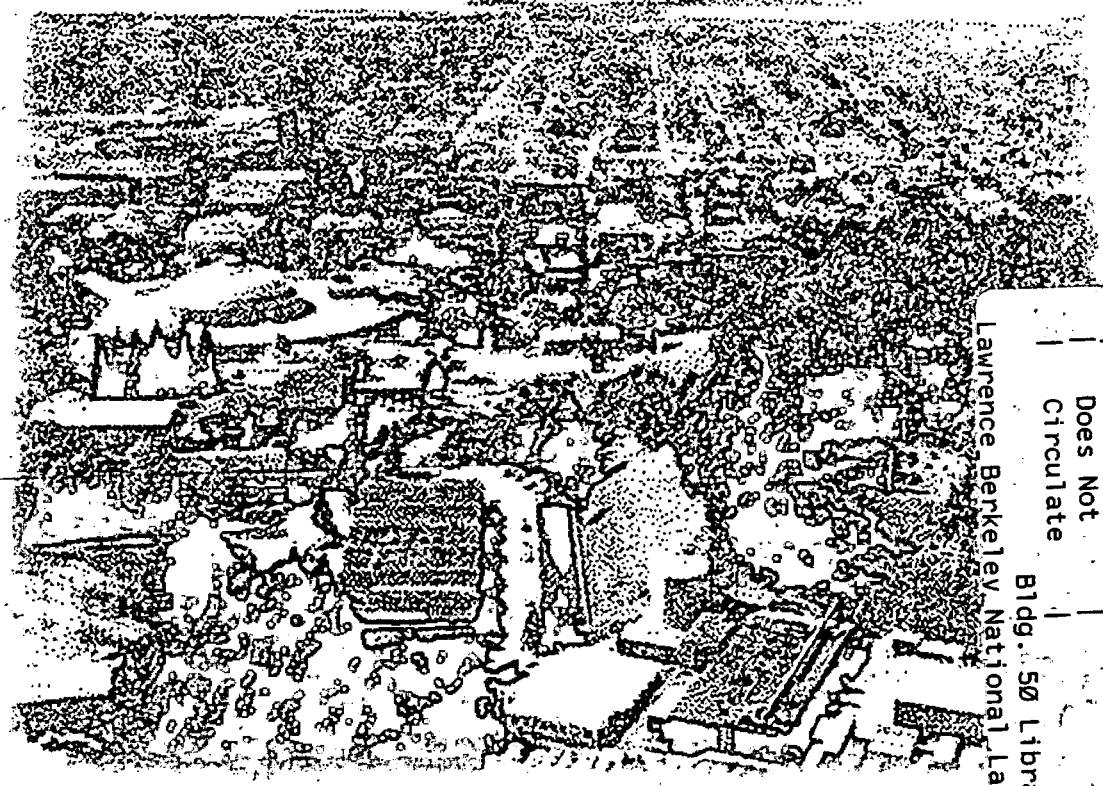

REFERENCE COPY
Does Not
Circulate
Bldg. 50 Library - Ref.
Lawrence Berkeley National Laboratory
LBNL-41854
Copy 1

DISCLAIMER

This document was prepared as an account of work sponsored by the United States Government. While this document is believed to contain correct information, neither the United States Government nor any agency thereof, nor the Regents of the University of California, nor any of their employees, makes any warranty, express or implied, or assumes any legal responsibility for the accuracy, completeness, or usefulness of any information, apparatus, product, or process disclosed, or represents that its use would not infringe privately owned rights. Reference herein to any specific commercial product, process, or service by its trade name, trademark, manufacturer, or otherwise, does not necessarily constitute or imply its endorsement, recommendation, or favoring by the United States Government or any agency thereof, or the Regents of the University of California. The views and opinions of authors expressed herein do not necessarily state or reflect those of the United States Government or any agency thereof or the Regents of the University of California.

LBNL-41854

Effect of Uniaxial Stress on Gallium, Beryllium, and Copper-doped Germanium Hole Population Inversion Lasers

Danielle Russell Chamberlin

Materials Sciences Division
Ernest Orlando Lawrence Berkeley National Laboratory
1 Cyclotron Road
Berkeley, California 94720

and

Materials Science and Mineral Engineering Department
University of California
Berkeley, California 94720

M.S. Thesis

May 1998

This work was supported by the DLR Institute for Space Sensor Research and the Director, Office of Energy Research, Materials Sciences Division, of the U.S. Department of Energy under Contract No. DE-AC03-76SF00098. DRC acknowledges support by fellowships from NASA Office of Space Science and UC Berkeley.

Effect of Uniaxial Stress on Gallium, Beryllium, and Copper-doped Germanium Hole Population Inversion Lasers

by

Danielle Russell Chamberlin

B.S. (Massachusetts Institute of Technology) 1996

A thesis submitted in partial satisfaction of the

requirements for the degree of

Master of Science

in

Engineering - Materials Science and Mineral Engineering

in the

GRADUATE DIVISION

of the

UNIVERSITY of CALIFORNIA at BERKELEY

Committee in Charge:

Prof. Eugene E. Haller, Chair
Prof. Eicke R. Weber
Prof. Paul McEuen

Spring 1998

Acknowledgments

I would like to thank Professor Eugene Haller for his continuous support and advice, and the time and effort he has put into supervising this project. The supportive environment that he provides for all his researchers truly has made this experience enjoyable.

I am very grateful for the scientific and non-technical advice Dr. Oscar Dubon provided throughout my first year at Berkeley. His supervision and strong support, along with his generous donation of time and effort to teach me, are greatly appreciated. Even more appreciated is his friendship.

In my second year at Berkeley it has been my pleasure to work with Dr. Erik Bründermann, an expert in the field of germanium far-infrared lasers. His vast knowledge has been an immense help and has greatly contributed to my understanding of this work.

There are many people who directly and indirectly contributed to this work, for which I am thankful. Ben Tang spent tedious hours preparing many of the lasers used in this study. Bill Hansen grew the germanium CZ crystals from which the lasers were fabricated. I am indebted to Jeff Beeman, Chris Olsen, and the other members of our group at LBNL for their technical and scientific advice. Their efforts have made a significant contribution to this work. Bill Knowlton, Marlene Almonte, and Dawnelle Wynne have provided the expert advice of senior students which is so essential to progress. With their advice these people have also provided friendships, for which I am truly grateful.

I am grateful to my husband Steve for his loving support of my studies, and my parents and family for providing me with a strong education.

I would also like to thank Professors Eicke Weber and Paul McEuen for reading this thesis and providing valuable input.

Finally, I would like to thank UC Berkeley and the NASA Office of Space Science for their support in funding my fellowship. This work was also supported by the DLR Institute for Space Sensor Research and the Director, Office of Energy Research, Materials Science Division, of the U. S. Department of Energy under Contract No. DE-AC03-76SF00098.

Table of Contents

1. Introduction 1
1.1 Motivation for research in p-Ge lasers 1
1.2 Other far-infrared lasers 2
1.3 Historical development of the p-Ge laser 3
1.3.1 Modes of laser emission 3
1.3.2 The emission gap 4
1.3.3 The push for continuous-wave 7
1.4 Mechanism of operation of the p-Ge laser 7
2. Effects of stress on p-type Ge: Theory 12
2.1 Band structure effects 12
2.2 Impurity effects 13
3. Effects of stress on p-type Ge: Experiments 19
3.1 Material growth and doping 19
3.2 Material characterization 20
3.3 Laser fabrication 21
3.4 Optical and electrical measurements 22
3.5 Uniaxial stress application 24
3.5.1 Prescale™ film calibration 24
3.5.2 Far-infrared absorption measurements 25
4. Ge:Ga Lasers 27
4.1 Previous stress measurements on Ge:Ga lasers 27
4.2 Lasing region - Ge:Ga 27
4.3 Effect of uniaxial stress 30
5. Ge:Be Lasers 35
5.1 Recent developments in Ge:Be lasers 35
5.2 Lasing region - Ge:Be 35
5.3 Effect of uniaxial stress 38
6. Ge:Cu Lasers 40
6.1 Motivation for using Ge:Cu 40
6.2 Lasing region - Ge:Cu 40
6.3 Effect of uniaxial stress 41
6.3.1 Results 41
6.3.2 Theoretical calculations 42
6.3.4 Explanation of results with theoretical calculations 44

7. Conclusions 47
7.1 Summary 47
7.2 Future Work 48
Appendix I: Streaming motion 50
I.1 Hole motion in a large electric field 50
I.2 Hole motion in crossed electric and magnetic fields 52
Appendix II: Pressure rig 56
References 61

1. Introduction

The germanium hole population inversion laser is a novel pulsed source of very far-infrared, coherent light. It is continuously tunable from 75 to 300 μm, and can emit powers of up to a few watts. It is unique in that it is the only semiconductor laser which is tunable over such a large frequency range. It is also the only semiconductor laser which emits in the very far-infrared. Although these are great achievements, successful applications for such a device still require deep investigation.

1.1 Motivation for research in *p*-Ge lasers

There are many applications where a far-infrared (FIR) laser is desirable, or even a necessity. Atmospheric and astronomical studies are frequently performed on far-infrared radiation sources. The resonant frequency of OH- ions studied in atmospheric ozone depletion is 2.5 THz, in the far-infrared energy region covered by the Ge laser. Molecules and ions present in star-forming regions also emit frequencies in the THz region, and far-infrared spectroscopy is often used to determine the composition of matter present in star burst galaxies.

It is difficult to find high-performance, low-noise electronics which operate at THz frequencies, which makes it troublesome to attain high resolution of far-infrared spectra. Heterodyne spectroscopy solves this problem by mixing incoming far-infrared light with a "local oscillator" in a non-linear device such as a hot-electron bolometer or Schottky diode. The non-linear device produces a signal frequency equal to the difference and the sum of the optical waves of the incoming light and the local oscillator. The difference signal can be placed conveniently in the GHz range, which is easily amplified and detected by modern electronics.

This far-infrared laser used as the local oscillator in heterodyne mixing spectroscopy needs to be continuously tunable and continuous-wave. Since the atmosphere absorbs many critical portions of the far-infrared spectrum, it is desirable to

operate a far-infrared spectrometer in space instead of within the earth's atmosphere. Current investigations above the troposphere include the European Space Agency's Infrared Space Observatory (ISO) and NASA's airborne observatory SOFIA (Stratospheric Observatory For Infrared Astronomy). Use on these platforms requires a laser to be small, light, continuous-wave, and rugged. The germanium laser fulfills all but one of these criteria: currently it is only operable in a pulsed mode.

1.2 Other far-infrared lasers

There are several other competitive sources of laser light which can be used for far-infrared spectroscopy. The free electron laser (FEL) is tunable over the entire far-infrared region from 30 to 1000 μm. However, it does not operate in continuous-wave mode and is too large to operate on a satellite or airborne observatory. In addition, FEL's normally have relatively wide linewidths, which is detrimental to high-resolution spectroscopy.

Gas, alcohol, and water vapor lasers have provided a means for heterodyne far-infrared spectroscopy for many years, but they have several shortcomings. First, they are non-tunable and emit at specific molecular rotational and vibrational frequencies. However, there are many lines throughout the range of interest and these can be widened with pressure, so reasonable spectral coverage can be attained. A more significant problem is that they must be optically pumped by large, powerful CO_2 lasers. This makes them useful for laboratory studies but not practical for operation in space.

The semiconductor multi-quantum well laser developed by Bell Labs has recently gained a lot of attention.[1] It has demonstrated CW optical power of 200 mW at operating temperatures of 80 K. However, the longest wavelength achieved is around 13 μm, placing it well outside the range of many far-infrared spectroscopic applications.

1.3 Historical development of the *p*-Ge laser

Studies of energy levels in bulk semiconductors under magnetic inductions have been conducted since the 1950's, and the possibility of population inversion between hole Landau levels was first postulated in 1955.[2,3] In 1972 Maeda and Kurosawa proposed a mechanism for achieving "a peculiar hot carrier distribution" by applying crossed magnetic and electric fields to a semiconductor.[4] Seven years later, Andronov, Kozlov, Mazov, and Shastin proposed that p-type germanium would be an appropriate material for achieving population inversion in this manner.[5] Spontaneous emission from inter-valence band transitions in p-type germanium was first seen by Komiyama in 1982 [6], and stimulated emission soon followed with Andronov's discovery in 1984.[7] Since then several types of emission have been found, and the effects of electric field, magnetic induction, and uniaxial stress magnitude have been investigated in detail. In the process of this investigation several questions arose which are now answered, but can appear perplexing if one looks only at the older literature. In the following sections, I will try to sort out these questions and provide an up-to-date understanding of the germanium FIR laser.

1.3.1 Modes of laser emission

The first germanium lasers which were discovered were found to operate based on transitions between the light and heavy-hole sub-bands.[7] Around the same time spontaneous [8] and stimulated [9] emission was also found to occur between light hole Landau levels at higher magnetic inductions. These two modes of emission were differentiated as "inter-valence band" and "cyclotron resonance" emission. The inter-valence band emission occurs at magnetic inductions around 1 Tesla and covers a broad-band spectrum. The cyclotron resonance emission occurs at magnetic inductions above about 2 Tesla and has a much narrower line width.

It is now understood that differentiating between these two modes is a

generalization. In a germanium crystal outside of a magnetic field, transitions between unmixed light and heavy hole bands are quantum-mechanically forbidden because holes in the light and heavy hole band have different angular moments. When a magnetic induction is applied, the germanium light and heavy hole valence bands split into Landau levels, with the amount of splitting proportional to the inverse effective mass. The heavy and light hole Landau levels cross and mix, and the resulting states have both light and heavy hole character. Because the light and heavy hole bands mix, the angular momentum of holes in these bands is not fixed and these transitions are allowed.

Population inversion occurs between the light and the heavy holes. This means that the emission occurs when a hole drops from a state which has more light hole character to a state which has more heavy hole character. The more mixed the final state is, the less defined is its energy. This increases the width of the emission band. The difference between inter-valence-band and cyclotron resonance emission refers merely the amount of mixing of the final state in the transition. At higher magnetic inductions, the splitting between Landau levels increases and the mixing between the light and heavy hole energy states decreases. This decreases the line width of the laser emission as the magnetic induction increases, and explains why the "cyclotron resonance" emission is seen only above 2 Tesla.

1.3.2 The emission gap

Fairly soon after the discovery of the gallium-doped germanium laser, Komiyama discovered that the emission was restricted to two wavelength regions.[10] At low magnetic inductions the laser emitted light in the range of 50 to 60 cm^{-1}, and at magnetic inductions above 0.55 T the laser emission was between 80 and 105 cm^{-1}. Upon application of uniaxial stress he found that the wavelength ranges broadened and emission occurred from 40 - 67 and 80 - 110 cm^{-1}.

To explain this emission gap, Komiyama calculated the probability of inter-band

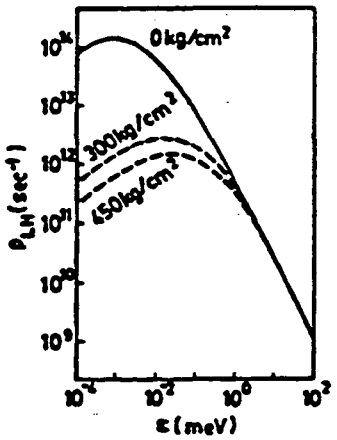

Figure 1-1: Calculated transition rate of light holes scattering into the heavy hole band from ionized impurities as a function of light hole energy and stress. (Courtesy Ref. [10])

impurity scattering as a function of light hole energy and uniaxial stress [Fig. 1-1]. This probability has a peak at low light hole energies and decreases with applied stress. At low hole energies, the carriers stay mainly near the Brioullin zone center. Here they need very little momentum change to scatter with an ionized impurity and go into the heavy hole band, and the probability of such a transition is rather high. At higher energies, if a hole encounters an ionized impurity, it will need both a significant momentum change and energy change to drop into the heavy hole band, so the probability of this transition drops.

Komiyama and Kuroda use an in-depth discussion of streaming motion [Appendix 1] to develop their theory of the emission gap. To summarize briefly, they suggest that at the optimum E and B conditions for lasing, light holes in a certain energy range will cross over the Brioullin zone center and have a high probability of scattering into the heavy hole band. Using this theory, Komiyama and Kuroda estimate that the energy gap should occur between 67 and 90 cm^{-1}, slightly off from the observed gap. With the application of uniaxial stress, the probability of a transition drops because the heavy and light hole bands split and a larger momentum change is now needed for a transition to occur. This was used to explain why the emission broadened with the

application of uniaxial stress.

There were several problems with Komiyama and Kuroda's theory. Their predicted emission gap of 67-90 cm^{-1} does not match up with that observed in emission spectra. In addition, their theory predicts that the emission gap should change with the ratio of E and B, but experiments show it to be invariant over all electric and magnetic induction conditions. A better explanation for the observed emission gap was offered by Kremser *et al.* [11] In their experiment they showed that the emission gap seen in the Ge:Ga laser matched exactly with the energies of the G, D, C, and B absorption lines of ground to excited-state transitions of gallium in germanium. To further prove their point, they compared the emission spectra of the Ge:Ga laser with a Tl-doped laser, and showed that the emission gap shifted in frequency.[12] In the Ge:Tl laser, the emission gap matched well with the G, D, and C lines of ground to excited-state transitions of Tl in germanium. They concluded that the emission gap was due to absorption of far-infrared photons inside the germanium crystal by neutral acceptors used to dope the material *p*-type.

Because the range of wavelengths in the emission gap are critical for many spectroscopic applications, there was interest in developing a laser that could emit throughout the entire far-infrared range. For this reason Bründermann *et al.* fabricated germanium lasers doped with the double acceptors beryllium and zinc. [13] Be and Zn have hole binding energies of 25 and 33 meV, respectively, much larger than 11 meV ionization energy of Ga in Ge. This leads to hole ground to excited-state transitions which have energies much higher than the emitted FIR photons. These lasers showed emission over the entire wavelength range of 75 to 300 μm.[14] Germanium lasers were also developed using the triple acceptor copper, which has an even larger ionization energy of 43 meV. These lasers also show laser emission throughout the range of the 120 - 170 μm gap. [15]

1.3.3 The push for continuous-wave

As stated before, for use in heterodyne spectroscopy the germanium laser needs to operate in a continuous-wave mode. The germanium laser must be pulsed because the large hole current necessary for operation heats the laser crystal. This heating increases the acoustic phonon density, which destroys the population inversion and the laser pulse. The first germanium lasers were made from large germanium crystals of dimensions about 50x5x4 mm^3. [7] The large volume of these lasers limited cooling during the pulse and kept the pulse length shorter than 6 μs and the duty cycle[1] around 10^{-5}.[29] In an effort to increase this duty cycle, a collaboration between DLR and UC Berkeley was initiated in 1996. Bründermann *et al.* used small lasers, with volumes of as little as 25 mm^3, to increase the relative cooling rate of the laser. [17] These small Ga and Al-doped laser crystals cooled much faster, leading to longer pulse lengths. Duty cycles as high as 1.5×10^{-4} were achieved, one order of magnitude better than the large laser crystals. By improving the heat sink that the lasers are mounted upon, the duty cycle of these lasers was increased by another order of magnitude to 2×10^{-3}. [18]

Further improvement has been made by using small lasers doped with the deep acceptors Be and Cu. The best duty cycle achieved with a Cu-doped laser has been 0.8 percent from a crystal doped 2×10^{15} cm^{-3} with dimensions 2.4x2.6x3.6 mm^3.[19] The present record duty cycle was reached with a Be-doped laser with dimensions 2x4x8 mm^3 and a doping level of 2×10^{13} cm^{-3}. [20] It is 2.5 percent at an emitted power on the order of a few milliwatts.

1.4 Mechanism of operation of the *p*-Ge laser

In germanium, as in all diamond-type structure semiconductors, there are three valence sub-bands, two of which are precisely degenerate at the minimum in energy at

---

[1]Duty cycle is the fraction of time that the laser is emitting light when it is operated in a pulsed mode, given by

duty cycle = repetition rate (Hz) x pulse length (s)

It is unitless. A duty cycle of one corresponds to continuous-wave operation.

the center of the Brillouin zone (see Fig. 1-2). The two degenerate bands are labeled the "heavy" and "light" hole bands according to their curvature. The third "split-off" valence band has a maximum much at lower electron energies (-290 meV below the top of the valence band) and does not play a significant role in free hole dynamics. At equilibrium, the relative density of states of the two valence sub-bands result in 96% of the holes lying in the heavy hole band and 4% of the holes occupying the light hole band. When an electric field is applied, the holes will accelerate in the direction of the electric field with very little energy loss until they reach the optical phonon energy. At this point they will emit an optical phonon and return to zero energy. This cycle of acceleration and energy loss by emission of a phonon is termed "streaming motion".[21][Appendix 1]

If a magnetic induction is now applied perpendicular to the electric field, the holes will feel a Lorentz force and undergo cyclical motion. Their velocity can be determined from the forces of the electric and magnetic inductions, as is shown in Appendix I. This gives an average hole velocity of $\sqrt{2}(E/B)$ and a maximum hole velocity of $2(E/B)$. This means the maximum hole kinetic energy at a fixed value of electric and magnetic induction is

$$E_{max} = 2m^*\left(\frac{E}{B}\right)^2. \tag{1.1}$$

Let us now consider the effect of the light and heavy hole bands. At low values of E/B, the holes will have very small kinetic energy and will not be able to reach the optical phonon energy. If we then raise the ratio of E to B, we will find a condition where the heavy holes can reach the optical phonon energy but the light holes cannot. This means the heavy holes will undergo streaming motion and emit phonons. When a phonon is emitted, the heavy hole has a 96% chance to stay in the heavy hole band and a 4% chance to go into the light hole band because of the relative density of states. If the hole does enter the light hole band, it will not have enough energy to emit an optical phonon. It will then stay in cyclical motion within the light hole band and have a relatively long lifetime. The light hole can now reenter the heavy hole band radiatively through

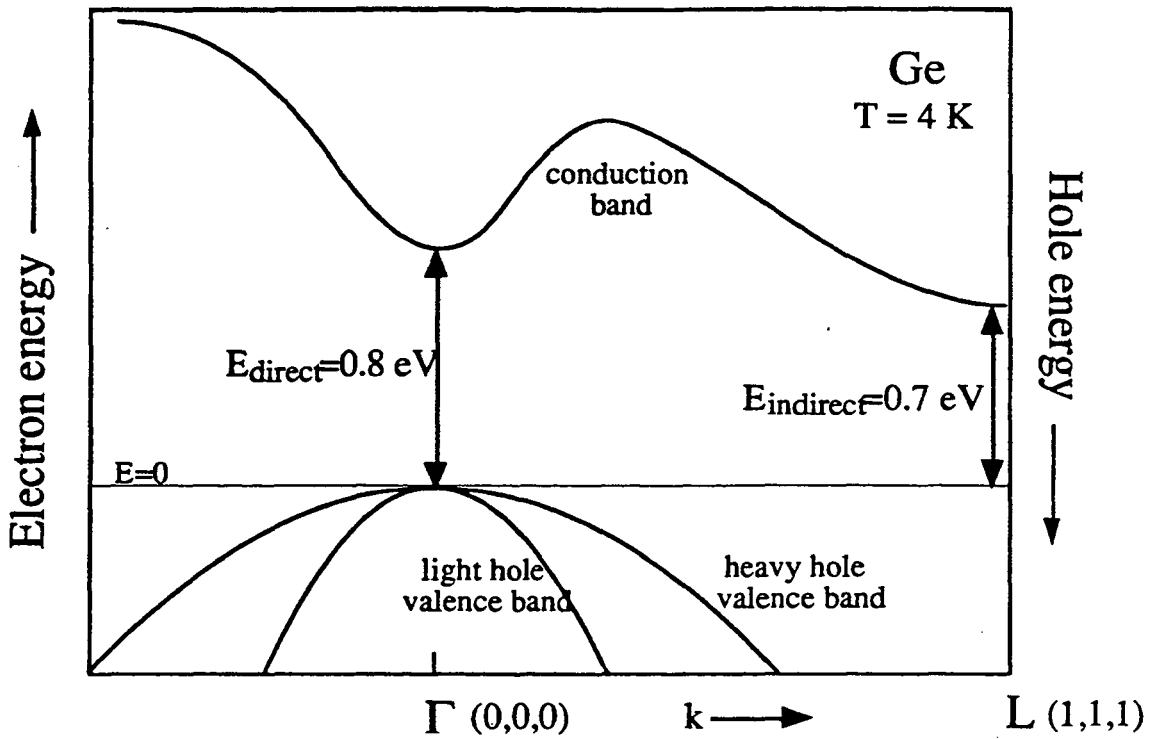

Figure 1-2: Schematic of the band structure of germanium

emission of a photon, giving rise to spontaneous emission. When many heavy holes enter the light hole band and accumulate there, a population inversion between the heavy and light hole bands occurs and stimulated emission occurs.

The magnetic induction has an additional effect: it splits the valence sub-bands into closely spaced Landau levels. In the free electron theory, the magnitude of the splitting is given by:

$$E_{splitting} = \left(v + \tfrac{1}{2}\right)\frac{\hbar eB}{m^* c} \tag{1.2}$$

where v is a quantum number running through all non-negative integers, $\hbar$ is Planck's constant over 2π, e is the charge on the electron, B is the magnitude of applied magnetic induction, c is the speed of light, and m^* is the effective mass of the energy band. Since the splitting is inversely proportional to the effective mass, the heavy hole Landau levels are spaced more closely than the light hole levels. As discussed in section 1.3.1, the light emission arises from radiative transitions between mixed light and heavy hole Landau

levels. Laser transitions occur from a less-mixed light hole state into a more-mixed light/heavy hole state. Because the magnitude of the splittings vary linearly with magnetic induction, the energy of the laser transition will increase with increased magnetic induction. Because of this the laser can be tuned over a large range of wavelengths.

The light holes can reenter the heavy hole band via two non-radiative methods: ionized impurity scattering and acoustic phonon scattering. Ionized impurity scattering is minimized by keeping the doping concentration low. To keep the light holes from losing energy by scattering with acoustic phonons, temperatures near that of liquid helium must be used. The probability of a hole scattering with a single phonon it encounters is linearly proportional to temperature given by the relation:

$$P \approx \left(\frac{m^*}{2\hbar k_h^2}\right)^2 \frac{k_B T \kappa}{V} \Xi^2 \tag{1.3}$$

where P is the probability of a scattering with an acoustic phonon, k_h is the electron wavevector, κ is the compressibility, V is the volume of the crystal, and Ξ is the deformation potential.[32] In addition, the population of phonons rises with temperature according to the Bose-Einstein phonon distribution function:

$$n_o = \frac{1}{\exp\left(\frac{\hbar\omega}{k_B T}\right) - 1} \tag{1.4}$$

where n_O is the number of phonons at energy $\hbar\omega$.[23] At low temperatures, the effects of inelastic scattering with acoustic phonons is low because both of these factors are low. When the temperature rises, the total probability increases to a significant amount. The light holes lose energy to acoustic phonons and reenter the heavy hole band, ruining the population inversion.

Unfortunately, at liquid helium temperatures practically all free holes freeze out onto neutral acceptors. To ionize these acceptors, a high electric field is needed. However, this high electric field also causes a high hole current. The high current causes

so much resistive heating in the crystal that after a few microseconds of light emission the crystal is too hot and lasing ceases. This is the only reason that the lasers must be pulsed to operate. In order to make progress towards continuous-wave operation, it is necessary to make the lasers more efficient, reduce the necessary current, and improve their cooling.

2. Effects of stress on *p*-type Ge: Theory

In order to study the mechanisms of laser action in the germanium laser, it is interesting to perturb the energy bands to see the effect on the lasing. A common way of changing energy bands is to apply a magnetic induction, however, the germanium laser already operates under a magnetic induction. A second way to change the band structure is to apply uniaxial stress. This chapter discusses the effects of uniaxial stress applied to on *p*-type germanium.

2.1 Band structure effects

The valence band of a diamond-type semiconductor contains two doubly-degenerate valence sub-bands, as described in section 1.4. The application of uniaxial stress causes a tetragonal distortion in the cubic lattice, breaking the cubic symmetry. This separates the $m_J=\pm 3/2$ states from the $m_J=\pm 1/2$ states and splits the light and heavy hole bands. In the k-direction of the applied uniaxial stress, the heavy hole band increases in energy relative to the light hole band and anticrossing occurs where they would overlap (see fig. 2-1, from [24]). This reduces the effective mass of the lower-energy band, which we will continue to consider to be the heavy hole band. Perpendicular to the direction of the stress no anticrossing occurs but the splitting is still apparent.

The decrease in the density of states effective mass was reported as a function of [001] stress in reference [25], and is shown in figure 2-2. These values were used as the heavy hole effective mass for the calculations in chapters four through six. Approximating the heavy hole mass using this value is reasonable because the density of states mass is 96% heavy and 4% light. It was also assumed that the light hole mass does not change significantly upon application of small [001] uniaxial stress. This is supported by results from cyclotron resonance experiments on uniaxially stressed *p*-type germanium [26].

This change in band structure can have several effects on the lasing action. First, it reduces the heavy hole effective mass, which will change the electric and magnetic induction conditions necessary for lasing to occur. Secondly, it splits the heavy and light hole bands, which will change the spacing between the energy levels and shift the wavelength of emission. This will also change the mixing of the light and heavy hole Landau levels such that the energy levels most favorable for population inversion may change. Splitting the heavy and light hole bands should also increase the light hole lifetime. The first and most obvious reason for longer lifetimes is that the splitting of the heavy and light hole bands will decrease the amount of tunneling from light holes into the heavy hole bands. However, tunneling is not the dominant cause of nonradiative transitions between the light and heavy hole sub-bands.[10] Ionized impurity scattering is the most probable nonradiative transition for light holes to enter the heavy hole bands, and is the limiting factor in the light hole lifetime. Under zero pressure, if a light hole interacts with an ionized impurity when it is near the Brioullin Zone center, it does not need a very large change in energy or momentum to enter the heavy hole band. When the sub-bands are split, the necessary momentum change for a scattering event to occur is increased. This decreases the probability for interband impurity scattering and increases the population inversion.

2.2 Impurity effects

The energies at which shallow, hydrogenic acceptor levels lie above the valence band is given by:

$$E_{acceptor} = 13.6 \frac{m^*}{m_e \varepsilon_r^2} \text{ eV} \qquad (2.1)$$

Where m^* is the density of states effective mass of the valence band, m_e is the free electron mass, and ε_r is the relative dielectric constant of the material. Since the two valence sub-bands split under uniaxial stress, the four-fold degenerate acceptor state will also split into two doubly degenerate energy levels. The remaining degeneracy in these

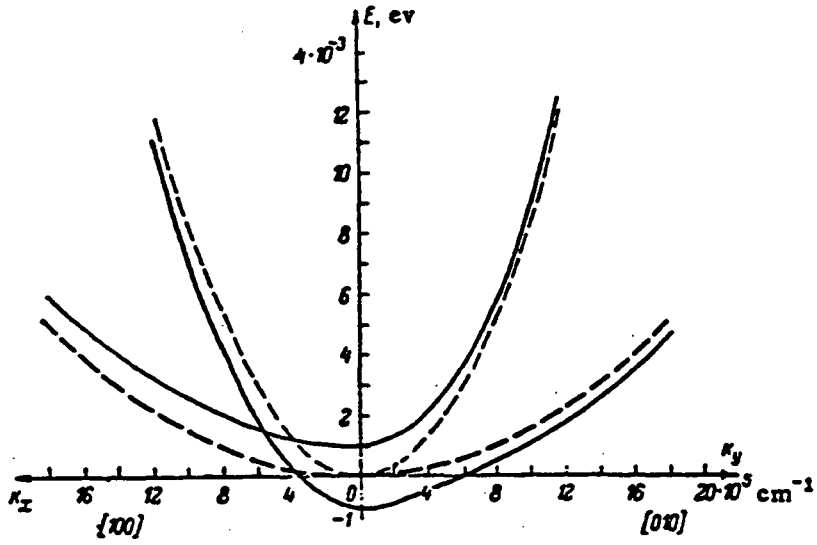

Figure 2-1: E vs. k of heavy and light hole bands under zero stress (dashed lines) and 0.33 kbar [100] stress (solid lines). Where the solid lines are shown to cross in this schematic, an anticrossing occurs. (Courtesy Ref. [24])

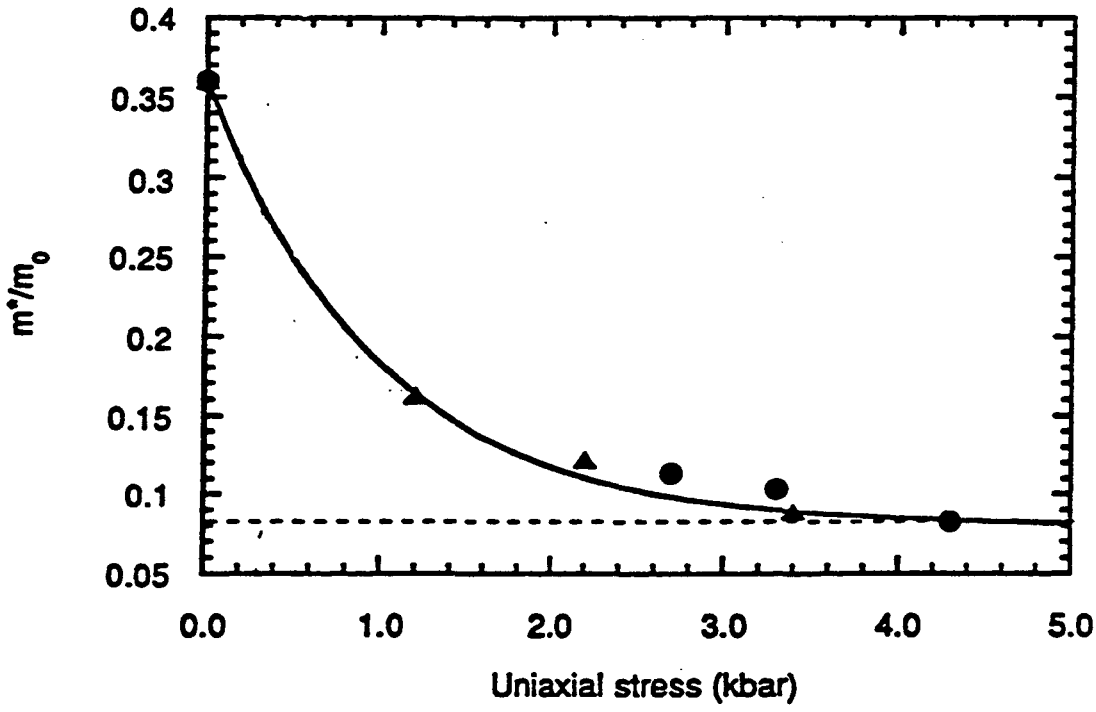

Figure 2-2: Density of states effective mass in germanium as a function of [100] uniaxial stress, as determined by photo-Hall effect measurements on Ge:Ga crystals with concentration 7×10^{11} cm^{-3} (triangles) and 3×10^{12} cm^{-3} (circles). (Courtesy Ref. [25])

levels is due spin and can only be lifted with the application of magnetic field. Because the effective mass changes with uniaxial stress, the ionization energy does not simply follow the splitting of the valence band. However, the magnitude of splitting in shallow acceptors has been theoretically determined, and observations from far-infrared absorption measurements agree well with the calculations. [27, 28] The splitting of the ionization energy is given by:[28]

$$\Delta'_{100} = 2b_X'(s_{11} - s_{12})T \tag{2.2}$$

$$\Delta'_{111} = \left(d'/\sqrt{3}\right)s_{44}T \tag{2.3}$$

Where Δ'_{xyz} is the splitting between the ionization energy levels when force is applied in the [xyz] direction, b' and d' are the deformation-potential constants for force applied along the [100] and [111] directions, respectively, s_{11}, s_{12}, and s_{44} are elastic compliance constants for germanium, and T is the magnitude of the uniaxial stress applied. The values of b' and d' are given in reference [27].

For double and triple acceptors such as Be and Cu equations 2.2 and 2.3 do not give the exact splitting energies. The trend of the ionization energy decreasing with applied stress still holds, but the value of the ionization energy must be experimentally determined through far-infrared absorption experiments.

In addition to the ground state energies, acceptors in germanium also have bound excited states similar to orbital energies of an atom or molecule. These lie at well-defined energies below the ionization energy and are labeled G, D, C, B, and A in order of increasing energy. The bound excited state energy levels split under uniaxial stress, just as the valence band and acceptor energy levels split. For shallow acceptors at in germanium at small stress the splitting follows the equations:

$$\Delta'_{100} = 2b_X'(s_{11} - s_{12})T \tag{2.4}$$

$$\Delta'_{111} = \left(d_X'/\sqrt{3}\right)s_{44}T \tag{2.5}$$

which are the same as equations 2.2 and 2.3 except the deformation-potential constants b' and d' for the ionization energy have been changed to new constants b_X' and d_X'. These

correspond to different deformation-potential constants for the bound excited states, where X denotes the bound excited state level (G, D, C, etc.). Values of these constants are given in reference [27].

As for the ionization energy, bound excited state energies of double and triple acceptors must be experimentally determined. The values of the excited-state energies for a number of multivalent acceptors under uniaxial stress can be found in references [29, 30]. Figure 2-3 is an example of such data from Ref. [29]. It is important to note that the bound excited state absorption peaks split into four lines under the application of uniaxial stress. This is because both the ground and bound excited states split, though by different amounts. With all combinations there are four possible ground-to-bound excited state transitions (figure 2-4). For shallow acceptors, these four transitions will have the energies

$$G_{[100]\,\text{stress}} = G_o \pm b'(s_{11} - s_{12})T \pm b'_G(s_{11} - s_{12})T \qquad (2.2)$$

for uniaxial stress in the [100] direction.

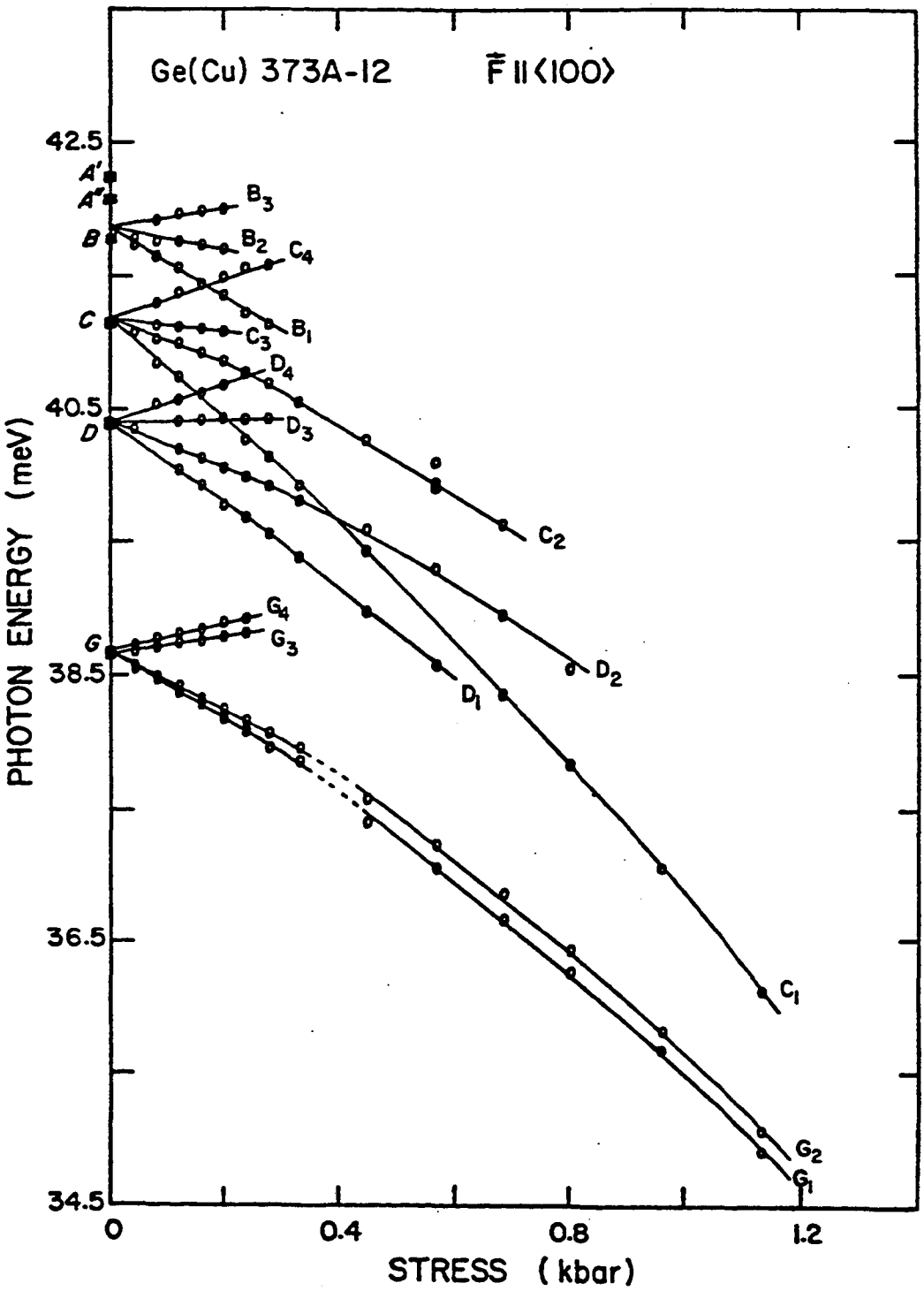

Figure 2-3: Bound excited state energies of copper in germanium as a function of [100] uniaxial stress. (Courtesy Ref. [29].)

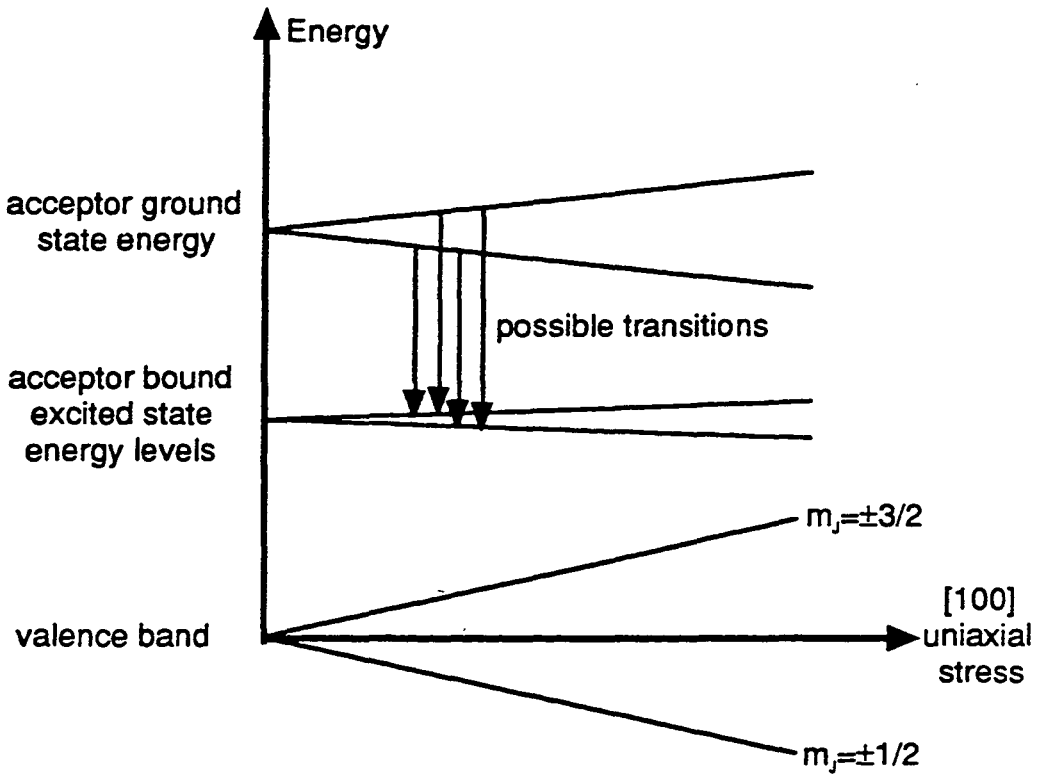

Figure 2-4: Schematic of the splitting of energy states in germanium under uniaxial stress. The four arrows show how the neutral acceptor ground state to bound excited state absorption lines split into four under the application of stress.

3. Effects of stress on *p*-type Ge: Experiments

3.1 Material growth and doping

For this study, bulk crystals of gallium, beryllium, and copper-doped germanium were used. Bulk crystals of gallium and beryllium-doped germanium were grown by the Czochralski method and lasers were fabricated from the as-grown material. Copper-doped germanium was obtained by diffusing copper into ultra-pure germanium grown by the Czochralski method. After the ultra-pure germanium growth, the material was characterized to determine the residual shallow acceptor concentration. The germanium crystal was then crystallographically oriented and a wafer of about 5 mm thickness was cut out with a diamond saw. The wafer was lapped with 600 and 1200 grit SiC powder/water slurries and then polish-etched in a 4:1 HNO_3: HF mixture.

Copper has a large diffusivity in germanium ($D=2\times10^{-7}$ cm^2s^{-1} at 700 °C [31]), which allows uniform doping with relatively short annealing times. Since the atom is so small, it diffuses by the "dissociative mechanism":

$$Cu_i + \text{vacancy} \leftrightarrow Cu_S \qquad (3.1)$$

The solubility of interstitial copper is much lower than that of substitutional copper, but it is far more mobile. For diffusion to occur, an interstitial copper atom diffuses through the crystal until it reacts with a vacancy and enters a substitutional site.

For the copper doping process, 1000 Å of copper was RF sputtered onto the wafer, and the crystal was sealed in a glass ampoule under vacuum. The thickness of copper film was determined to be in excess of that needed to achieve the desired doping concentration: a back of the envelope calculation shows that this thickness provides 10^{17} cm^{-3} copper atoms inside the germanium crystal. The germanium was then annealed at 700 °C for 24 hours for complete diffusion to occur. The ampoule was then rapidly quenched in ethylene glycol. This "freezes" the copper atoms on their equilibrium sites at the annealing temperature, so the concentration of electrically active copper will be close

to the concentration of substitutional copper at 700 °C.

3.2 Material characterization

After growth the germanium crystals were characterized for dopant type and concentration by variable-temperature Hall effect. Because of impurity segregation a CZ-grown crystal will have dopant concentration change along its length, so care was taken to measure the concentration of the very wafer from which the lasers were obtained. The germanium used for copper doping was measured before annealing to determine the residual shallow acceptor concentration and type in addition to the compensation level. After annealing a room-temperature measurement was performed to determine the concentration of electrically active copper.

In a Hall effect measurement an electric field is applied perpendicular to a magnetic induction, which by the Lorentz force creates an internal electric field within the crystal. This so-called "Hall field" is given by:

$$E_{\text{Hall}} = \frac{J_E B}{N_c e} \tag{3.2}$$

where B is the applied magnetic induction, J_E is the current density in the direction of the applied electric field, e is the charge on the electron, and N_C is the number of free carriers. By measuring the voltage created perpendicular to the applied magnetic and electric fields, one can determine the free carrier concentration. The direction of the Hall field also determines whether the material is n- or p-type.

By measuring the Hall field as a function of temperature, we can determine the freeze-out curve for the majority carrier in the semiconductor [figure 3-1]. This figure shows two freeze-out regions corresponding to freeze-out of two different acceptors with differing ionization energies. The higher and lower plateaus in the curve give the concentration of copper and shallow acceptors, respectively. If the compensation with donors were very low there would be two distinct slopes to the shallow acceptor freeze-out portion of the log concentration-inverse absolute temperature plot. The higher-

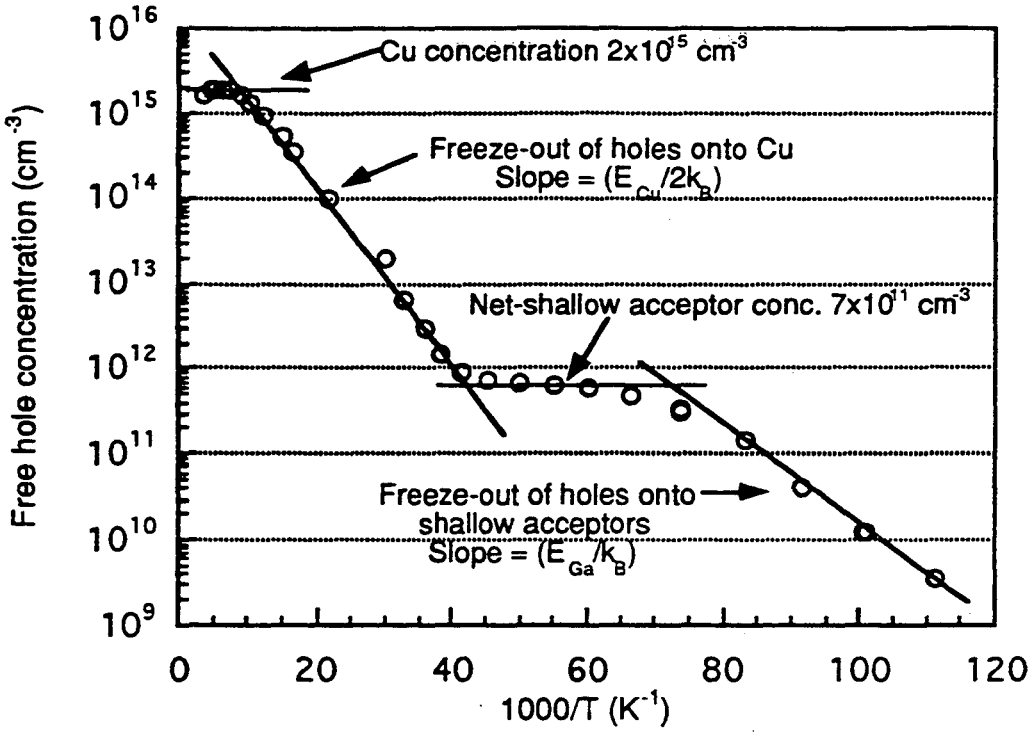

Figure 3-1: Freeze-out curve of ultra-pure germanium annealed with a copper film at 700 °C, as determined by variable-temperature Hall effect.

temperature slope would have the value $E_a/2k_B$ and the lower-temperature slope would have the value E_a/k_B, where E_a is the ionization energy of the majority impurity. The freeze-out of the shallow acceptor portion in figure 3-1 shows only the full shallow acceptor ionization slope E_a/k_B which indicates that the compensating donor concentration is of the order of 10^{11} cm^{-3}. By measuring this slope we can determine the average acceptor ionization energy.

3.3 Laser fabrication

A germanium laser consists simply of a *p*-type germanium crystal with electrical contacts on two opposing faces. To fabricate these, Czochralski-grown crystals were cut with an ID saw into wafers of a desired thickness, usually 5 mm. This thickness is determined by the desired distance between the electrical contacts. The surfaces of the

wafers were then lapped with 600 and 1200 grit SiC-water slurry and polish-etched in a solution of 4:1 HNO_3: HF mixture. To create electrical contacts, boron was implanted into two opposing faces of the wafer. The boron doses used were $1x10^{14}$ and $2x10^{14}$ cm^{-2} at 33 and 50 keV, respectively. After implantation the wafers were etched for 15 seconds in HF to remove any surface oxide and placed immediately under vacuum in an RF sputtering machine. Both sides of the wafer were sputtered with 400 Å of Pd and 4000 Å of Au. Post-implant annealing was then performed at 300 °C for 1 hour under N_2 ambient to remove implant damage and fully activate the boron.

After electrical contacts were fabricated, the wafers were crystallographically oriented by looking at the facets on their edges, and cut into the desired laser sizes. This method produces crystals which are oriented to within less than a degree of the desired direction, and produces surfaces parallel within 30 arcseconds. The cut surfaces were then lapped with 600 and 1200 grit SiC slurry to remove saw damage, and polish-etched in a solution of 7:2:1 HNO_3: HF: fuming HNO_3 mixture. The mirror-like quality of these surfaces is critical to laser performance, since no external resonators are used.

Table 3-1 lists the germanium crystals which were fabricated for use in these experiments, their doping levels, sizes, and orientations. The crystal number references the germanium CZ crystal from which the laser was cut. In the case of the copper-doped lasers, the diffusion temperature is also given. In the case of the Ga and Be-doped lasers, the length from the seed at which the Ge wafer was cut is listed.

3.4 Optical and electrical measurements

Laser crystals were mounted between two copper plates which served both as electrical leads and cooling plates. In the pressure rig, the top plate was replaced by a brass piston which applied uniaxial stress as well as providing electrical contact. The laser crystals were then placed at the end of a long light pipe made of non-magnetic stainless steel and inside of a liquid helium cryostat. Inside the cryostat and surrounding the laser crystal was a Cryomagnetics superconducting magnet capable of producing up

Ge crystal number	Laser number	Orientation E, P x B, light x other	Size (mm)	Dopant	Conc. (cm^{-3})
745-700°C	D01	<100>x<110>x <110>	5.0 x 3.7 x 2.8	Cu	$3x10^{15}$
745-700°C	D04	<100>x<110>x <110>	4.6 x 2 x 2	Cu	$1x10^{15}$
760-12.4	D06	<100>x<110>x <110>	4.0 x 3.3 x 2.9	Ga	$8x10^{13}$
755-12.0	D07	<111>x<110>x <112>	2.6 x 3.9 x 2.9	Ga	$3.5x10^{13}$
854-2.2	D09	<100>x<110>x <110>	5.2 x 3.4 x 3.0	Be	$1x10^{14}$

Table 3-1: List of crystals fabricated

to 9 Tesla of magnetic induction. A Ge:Ga photoconductor was placed inside the light pipe to detect the far-infrared light.

The electrical leads connected to the laser crystal were connected to a custom-made pulse generator consisting of a large capacitor and high voltage, high current solid state switches. This pulse generator is capable of producing pulses of several kilovolts with currents as high as 100 A, pulse lengths as short as 100 ns, and frequencies as high as 100 kHz. The high voltage for this pulse generator was supplied by a Northeast Scientific RE3002EW high voltage power supply capable of producing up to 2.5 kV. The electric field in the laser crystal was estimated to be the voltage across the capacitor divided by the distance between electrical contacts on the laser crystal. The actual voltage across the crystal was smaller than this value because of resistive losses in the two meter long current leads, however this difference is considered to be insignificant.

The current for the superconducting magnet was supplied by a HP 6260 DC power supply, and regulated by a Cryomagnetics Model 30 Persistent Switch and Model 60 Programmer/Monitor. The magnitude of magnetic induction in Tesla was determined by multiplying the current reading on the Model 60 Programmer/Monitor by a factor of 0.1168.

The voltage across the Ge:Ga photoconductor was monitored on a Tektronix

Model 640A 4 Channel, 2 GHz Digitizing Oscilloscope. The oscilloscope was triggered by the voltage pulse from the pulse generator, and the voltage across the capacitor and the current through the laser crystal were monitored in the oscilloscope as well. The values of electric field, current through the laser crystal, and relative intensity of the laser pulse were measured at the onset, peak, and end of lasing as electric field was increased at a set magnetic induction. The magnetic induction was scanned from 0.5 to 2.5 Tesla to determine the limits of electric and magnetic inductions necessary for laser operation.

3.5 Uniaxial stress application

In order to apply uniaxial stress to the laser crystal, a new holder for lasers had to be fabricated. This holder had the constraints of needing to apply up to 500 bar of pressure on a 10 mm^2 sample perpendicular to the magnetic induction direction and within a cryostat at 4 Kelvin. In addition, it was desirable to be able to alter the stress from outside of the cryostat without removing the laser from the liquid helium, since a few liters are lost each time the laser is removed and placed back inside the cryostat. Since the magnet has a 1" bore, the entire mechanism must fit inside a cylinder less than 1" in diameter. These constraints severely limited the design of the pressure apparatus. The resulting pressure rig is described in detail in Appendix 2.

3.5.1 Prescale™ film calibration

The uniformity and magnitude of the pressure applied was determined by placing a small piece of Fuji HS-grade Prescale™ film between the brass piston and the laser crystal. This method has been used in previous studies of uniaxially stressed germanium lasers.[10] This film is coated with liquid crystals which change color to pink with pressure applied. The density of the pink color can be matched to a calibration chart provided with the film and the pressure can be estimated from this value. During calibration pressure was applied and released at room temperature. The film was

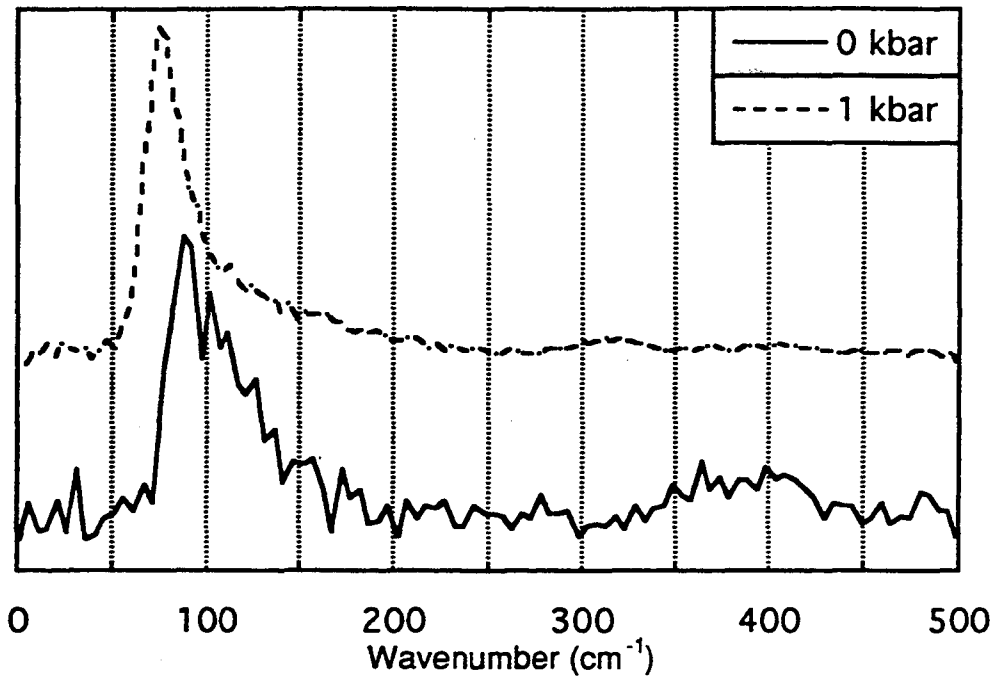

Figure 3-2: Far-infrared absorption of Ge doped with 10^{15} cm^{-3} Cu. Dotted line- residual pressure, solid line - 1 kbar pressure applied parallel to [001]

removed without moving the laser crystal and the piston put back in place. The pressure was then reapplied for laser operation exactly as during the pressure measurement. From visual observation of the Prescale™ film it was possible to determine that the pressure was very close to that expected from the known force applied to the crystal. In addition, the pressure uniformity could be estimated from the variation in intensity of the film color. If the pressure was applied only to a small portion of the laser crystal, the piston was sanded or the bottom copper contact flattened until the pressure uniformity looked reasonable. However, this is not a sensitive technique and it is likely that the pressure still had significant variation.

3.5.2 Far-infrared absorption measurements

The magnitude and uniformity of the pressure were also confirmed by a far-infrared absorption measurement. Far-infrared light from a Michelson interferometer was

sent into crystal D04 and the conductivity was determined as a function of wavenumber. Measurements were taken with residual pressure and 1 kbar of pressure in the [001] direction. The crystal used for the absorption measurement had a 4 mm^2 cross-section, much smaller than the 10 mm^2 cross-section used for laser crystals. This allowed higher pressure to be reached and significant shifting of the energy peaks could be seen. The results are shown in Figure 3-2. We expect to see a peak due to copper impurities at 43 meV or around 350 cm^{-1}. This peak is small compared to the absorption from residual shallow impurities in the zero-stress measurement, and it completely disappears at higher pressures. The stressed crystal (solid line) shows a shift of the shallow-acceptor absorption edge from 89 cm^{-1} or 11 meV to 75 cm^{-1} or 9.3 meV. From measurements of the ionization energy of gallium with uniaxial stress, we can determine that this shift corresponds to a pressure of about 1.1 kbar, which is very close to the estimated applied pressure of 1 kbar.[25]

Although we have achieved the pressure we desire, we see that the peaks broaden significantly or disappear completely upon application of stress. This means that the pressure uniformity is not very high. Since this technique is much more sensitive than the Prescale™ film measurement, it is not unreasonable to find a significant pressure distribution that was not observed by the film. It is estimated from the two pressure calibration techniques that the variation in pressure throughout the laser crystal could about 30%. However, since the absorption peaks shift very close to what is expected, it is assumed that the average pressure applied to the crystal is the same as the magnitude of the pressure set by the stress rig to within 10%.

4. Ge:Ga Lasers

4.1 Previous stress measurements on Ge:Ga lasers

Because uniaxial stress changes the band structure as described in chapter 2, the effect of pressure on the lasing region was investigated very soon after germanium lasers were invented. The first study of the effects of uniaxial stress on p-Ge hot-hole lasers was conducted by Komiyama and Kuroda in 1988. [10] They applied compressive stresses of 300 and 450 bar along the [112] direction of a Ge:Ga crystal, parallel to the electric field. Under uniaxial stress they saw a reduction in the resistivity of the crystal and the breakdown voltage needed to impact ionize the acceptors. This is as expected, since a compressive force is known to decrease the ionization energy of acceptors (section 2.2). The intensity of the laser increased, and the critical electric field and magnetic induction at which lasing started was observed to decrease. This was attributed to a decrease in ionized impurity scattering between the two bands, as described in section 1.3.2.

Gavrilenko and co-workers later published a series of experiments designed to investigate the intervalence band emission with applied pressure. [32, 33] Pressure was applied parallel to B in a [110] direction. They also saw a decrease in the critical electric and magnetic inductions necessary for lasing to occur. It was observed that the laser intensity did not increase linearly with pressure, as would be expected if decreased ionized impurity scattering were the only effect causing the increased population inversion. From this observation they concluded that a reduction in intersubband tunneling also plays a role in stressed lasers.

4.2 Lasing region - Ge:Ga

Even though previous results on stressed Ge:Ga lasers have been published, devices were fabricated from this material and studied to provide a thorough and direct

comparison to the Ge:Be and Ge:Cu results. Ga-doped lasers D06 and D07 were measured to test the effect of crystallographic orientation. Most lasers tested, like D06, were oriented with electric field and pressure in the [001] direction, where the valence band splitting is the largest. Because previous studies used other orientations, one laser (D07) was made with orientation <111> x <110> x <112> to compare to Komiyama's results. Magnetic induction was set at a constant value, and the electric field was scanned from zero to 2 kV cm^{-1}. Data of the electric field values were taken at the onset and end of lasing. The magnetic induction was varied from 0.4 to 2.5 Tesla, and the critical values of electric and magnetic inductions necessary for lasing were plotted.

The zero-stress results for lasers D06 and D07 are shown in Figure 4-1. The conditions for which lasing is seen are given by the oval-shaped areas inside the dotted lines. The minimum theoretical limit (solid line) is calculated from equation 1.1

$$E_{max} = 2m^* \left(\frac{E}{B}\right)^2 \qquad (1.1)$$

and corresponds to the E/B ratio where the heavy holes reach the optical phonon energy of 37.2 meV. The maximum theoretical limit (dashed line) is calculated using the energy at which the maximum light hole energy reaches 37.2 meV. There is a dividing line between the areas in which the two lasers operate at E/B = 1.2 kV cm^{-1} T^{-1}. D07, the crystal oriented with electric field parallel to the [111] direction, operates only at E/B < 1.2 and D06, with electric field parallel to the [001] direction, operates only at E/B greater than this critical number.

Figure 4-2 shows the calculated heavy and light hole energies as a function of E/B. This graphically illustrates the maximum and minimum limits for lasing. When the maximum heavy hole energy exceeds the optical phonon energy, at E/B of 0.95 kV cm^{-1} T^{-1}, lasing can occur. The maximum limit for lasing is seen when the light holes reach the optical phonon energy at E/B = 2.75 and return to the heavy hole band, ruining the population inversion.

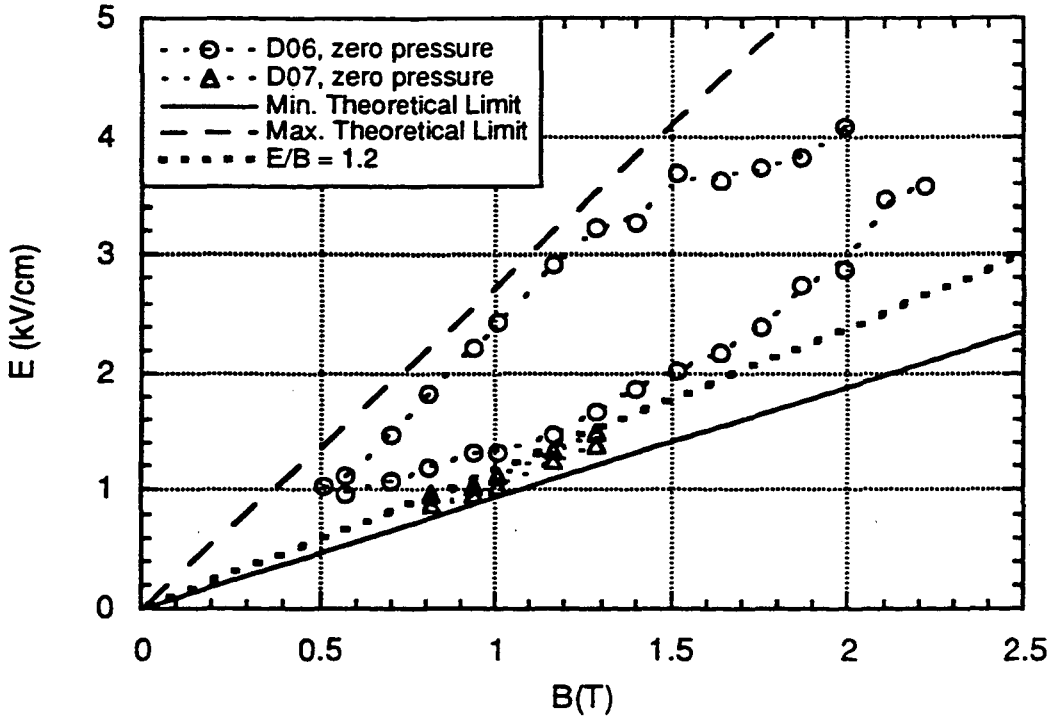

Figure 4-1: Electric field and magnetic induction conditions for lasing to be observed in Ge:Ga crystals. Crystal orientation: D06 - E//<001>, B//light//<110>, D07 - E//<111>, B//light//<110>.

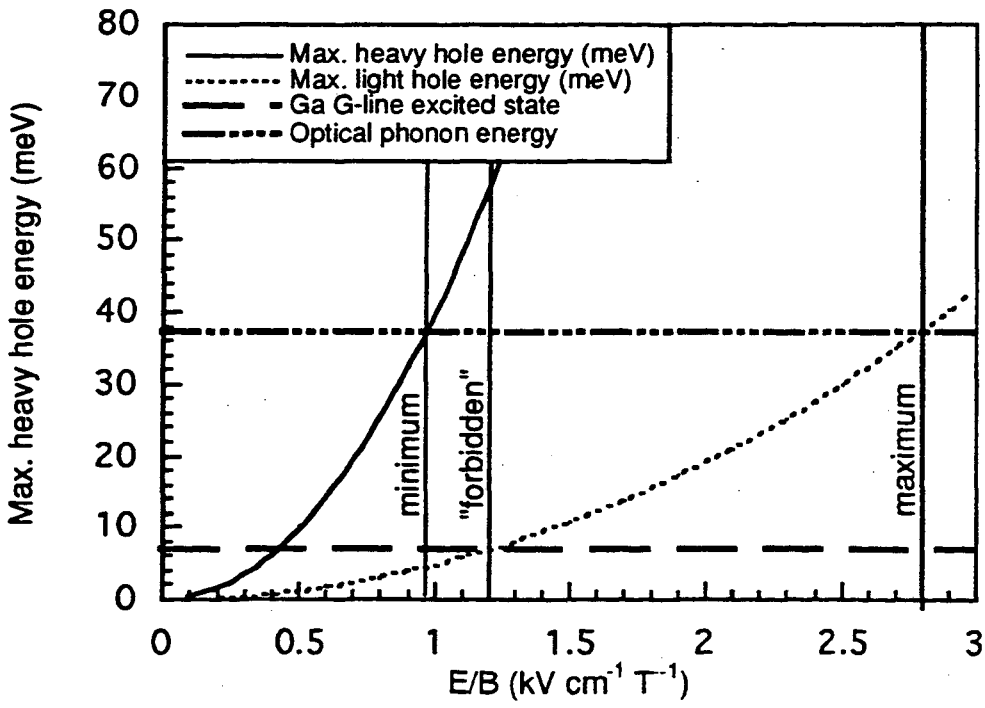

Figure 4-2: Calculated energies of heavy and light holes at zero stress as a function of E/B.

Lasing is not seen in either crystal at E/B = 1.2 kV cm^{-1} T^{-1}. In Figure 4-2 we can see that this is the condition at which the light holes have the same energy as the lowest ground-to-bound excited state transition of neutral gallium in germanium. From this observation we can propose that at this E/B ratio, light holes transfer their energy to a neutral gallium, which will then excite a hole into a bound excited state. The light hole will return to zero energy, with a 96% probability of entering the heavy hole band. This decreases the population inversion. Hence we see no lasing in either crystal at E/B = 1.2 kV cm^{-1} T^{-1}. It is important to note that other studies have observed lasing from crystals at E/B = 1.2 kV cm^{-1} T^{-1} and much larger E-B regions of emission overall. However, they have used much larger crystals and/or external resonators which improve the gain tremendously.

Because of the varying band structure in different crystallographic directions, the Landau level splitting will vary with different *E* and *B* orientations. Landau levels in differently oriented crystals will occur at different energies, and therefore the probability of stimulated emission as a function of B will be stronger in certain orientations. [16] Although Ref. [16] does not calculate the probabilities for both orientations chosen in this study, it does show that certain orientations exhibit stronger lasing at high E/B and others will lase more strongly at low E/B. Since the gain in these laser crystals is low to begin with, we can expect lasing only where the population inversion is very strong. Thus it is reasonable that D07 does not exhibit lasing at E/B > 1.2 kV cm^{-1} T^{-1} and D06 operates only in this region.

4.3 Effect of uniaxial stress

Figure 4-3 shows the effect of applying 300 bar of uniaxial stress in the [001] direction on laser D06. Lasing occurs over a smaller range of *E* and *B* and at the lowest E and B values lasing ceases altogether. The lasing also ceases at the high-field conditions. This is directly contrary to the increase in low-field operation seen by Komiyama *et al*

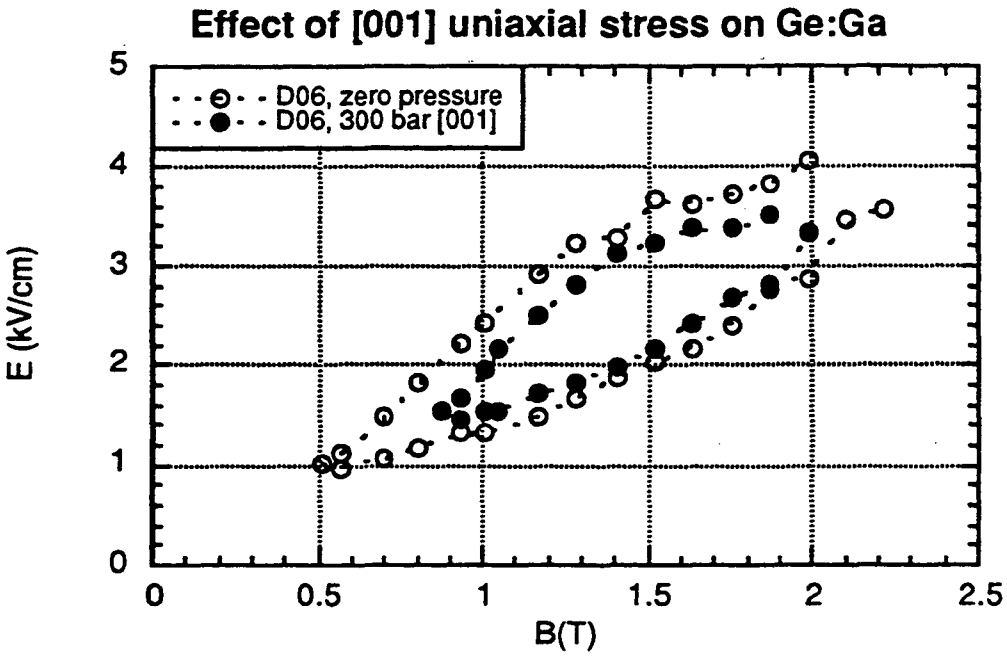

Figure 4-3 Electric and magnetic induction conditions for lasing to be observed in Ge:Ga crystal D06 at residual pressure (< 20 bar) and under uniaxial stress of 300 bar in the [001] direction parallel to the electric field.[10] and Gavrilenko *et al.* [32, 33]

The decrease can be understood because the uniaxial stress decreases the effective mass of the heavy holes from a value of 0.35 m_0 at zero stress to 0.28 m_0 at 300 bar, as discussed in section 2.1 and shown in table 4-1. This means it will take a larger electric field at a given magnetic induction to accelerate the heavy holes up to the optical phonon energy. The 0.3 kbar stress increases the minimum E/B condition for lasing from 0.966 $kVcm^{-1}T^{-1}$ to 1.080 $kVcm^{-1}T^{-1}$. This decreases the population inversion overall and thereby shrinks the lasing zone. At the lowest and highest fields where the inversion was not strong in the stress-free condition, the lasing is completely absent in the stressed condition.

Stress	Optical Phonon Energy (meV)	heavy hole m* [25]	light hole m*	minimum E/B ($kV\ cm^{-1}T^{-1}$)	maximum E/B ($kV\ cm^{-1}T^{-1}$)
0 bar	37.2	0.35 m_0	0.042 m_0	0.966	2.789
300 bar	37.2	0.28 m_0	0.042 m_0	1.080	2.789

Table 4-1: Effect of stress on variables in and solutions to equation 1-1.

The effect of stress on crystal D07 was also investigated to determine whether the difference between these stress results and the literature could be due to a difference in orientation. As the stress was increased to 400 bar, the laser intensity dropped quickly and no lasing was seen above a stress of only 100 bar. To explain this, we will try to recalculate the E/B limits for lasing under uniaxial stress. The pressure decreases the energy of the lowest Ge:Ga G-line [27], which will decrease the upper E/B limit at which the light holes transfer their energy to neutral acceptors. The splittings of the G-line energies for shallow acceptors have been theoretically determined, and the energy of the lowest ground-to-excited state G transition can be calculated from the equation: [28]

$$G_{[111]\,\mathrm{stress}} = G_o - 0.288d' s_{44}T - 0.288d'_G s_{44}T \qquad (4.1)$$

Where G_O is the energy of the G-line at zero stress, d' is the deformation-potential constant for the ground state, d_G' is the deformation-potential constant for the G excited state, s_{44} is an elastic compliance constant, and T is the applied uniaxial stress. Using the values of these constants from references [26, 27] we obtain an energy for the lowest G-state of 6.5 meV at 300 bar [111] uniaxial stress. This small change in the G energy should only decrease the E/B ratio to about 1.17 kV cm^{-1} T^{-1} at 300 bar, so it does not explain the total lack of lasing at pressures as low as 100 bar. The minimum E/B for lasing increases about 10% under [001] uniaxial stress (table 4-1.) We do not know the effect of [111] stress on the heavy hole effective mass, but it should not be as large as the [001] stress-induced change since the spitting in the [111] direction is not as large. This means the change in the lower limit for lasing should be less than 10% for crystal D07.

Although the average stresses applied are very small, it is likely that the uniformity is poor and there may be certain regions in the crystal where the stresses are large. This means that as soon as a small stress is applied, there will be certain areas with high enough stress so the upper and lower limits for lasing coincide. Ninety-six percent of the holes in this area of the crystal will occupy the heavy hole band. Since the population inversion is weak in crystal D07 to begin with, this local area of equilibrium

population will cause lasing to vanish completely.

It is necessary to reconcile the detrimental effect of pressure shown here with the Komiyama and Gavrilenko papers. In the papers of Gavrilenko *et al* the laser zone is not very large to begin with and does not come close to the theoretical limits.[32, 33] This is probably due to a high dopant compensation level leading to significant ionized impurity scattering, which shortens the light hole lifetime and decreases the population inversion. Uniaxial stress would decrease the ionized impurity scattering as described in the paper and thereby increase the laser zone.

Unfortunately, Gavrilenko's papers do not explicitly state what the actual compensation level in their crystals is. In one version of the paper the germanium is described as "low compensated Ge:Ga ($p = 5x10^{13}$ cm^{-3})" but the actual compensation level is not stated. In another preprint version of the same paper, the crystals are stated to be "low doped Ge:Ga ($N_a - N_d = 5x10^{13}$ cm^{-3}, $N_a/N_d \leq 0.5$)". Clearly there is some confusion here, because the acceptor-to-donor ratio stated in the preprint makes the germanium n-type! If we guess that the ratio should be flipped, this does not give us a very good compensation level.

Komiyama and Kuroda do not state their compensation level at all.[10] Their lasing zone is much larger than that seen by Gavrilenko *et al.*, but this may be due to large gain from good mirrors instead of a lack of ionized impurities. The increase in lasing with stress is then, as they describe, a decrease in ionized impurity scattering.

The germanium crystals grown for these experiments had low compensation. In the crystal used for laser D06, variable-temperature Hall effect was used to determine that the concentration of compensating donors was about $3x10^{12}$ cm^{-3}. This gives a compensation ratio N_d/N_a of 0.0375, most likely a much lower compensation level than those encountered in the crystals used in the other studies. Because in this study there are very few ionized impurities to begin with, the decrease in ionized impurity scattering with applied uniaxial stress does not play a major role in determining the laser

characteristics. With low-compensated germanium the effect of uniaxial stress is merely to change the band structure and the effective masses, which changes the conditions for lasing to occur. Without many ionized impurities, the light hole lifetime does not rapidly increase upon the application of stress.

5. Ge:Be Lasers

5.1 Recent developments in Ge:Be lasers

Because the neutral gallium in Ge:Ga lasers absorbs light, our group at LBNL has developed and studied germanium doped with the deeper acceptors beryllium, zinc, and copper. As described in section 1.3.2, lasers doped with these acceptors show full tunability over the entire range of 75 to 300 μm. The beryllium-doped germanium lasers also operate at different E/B ratios than those seen in the shallow-doped lasers. The heavy hole energy at the lowest E/B ratio where lasing is observed can be computed from equation 1.1. In shallow acceptor-doped lasers this energy coincides with the optical phonon energy. [6] In beryllium-doped germanium lasers, lasing is observed at values of E/B where the heavy holes do not have enough energy to scatter with optical phonons. [13] However, the heavy hole energies at which the onset of lasing is observed coincide with the lowest, optically active ground-to-bound excited state transition of neutral beryllium acceptors in germanium (the G line). The exact mechanism by which inversion is achieved is not completely understood. However, it is proposed that heavy holes inelastically scatter with neutral beryllium impurities, giving up their energy and momentum. The heavy hole returns to zero energy, with a 4% chance of entering the light hole band. The neutral beryllium impurity excites hole into a bound excited state, which then either absorbs a phonon and is promoted into the valence band or returns to the ground state by emission of acoustic phonons.

5.2 Lasing region - Ge:Be

A beryllium-doped laser D09 with similar size and doping level to the gallium-doped laser D06 was tested to compare the lasing region differences of the two differently-doped materials. The result is shown in figure 5-1. At the same magnetic induction the Ge:Be crystal lases at lower electric fields than the Ge:Ga crystal. This is

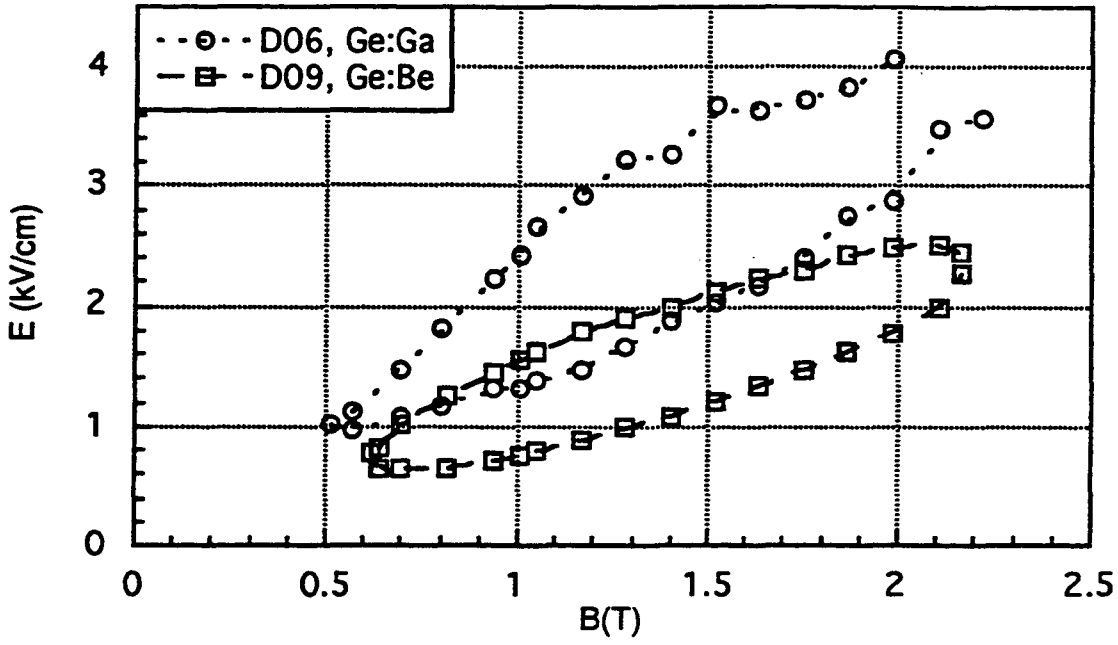

Figure 5-1: Comparison of electric field and magnetic induction conditions necessary for lasing in similar concentration, size, and oriented crystals of Ge:Be (D09) and Ge:Ga (D06).

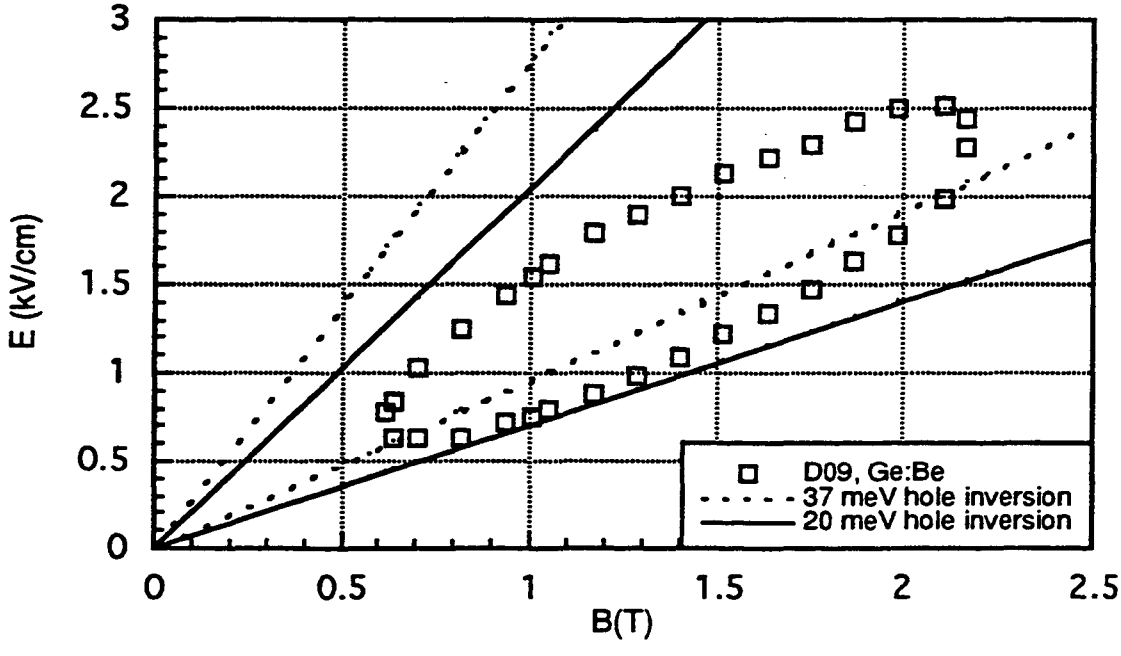

Figure 5-2: E and B-field conditions necessary for lasing in Ge:Be laser D09, with calculated theoretical limits from two inversion mechanisms.

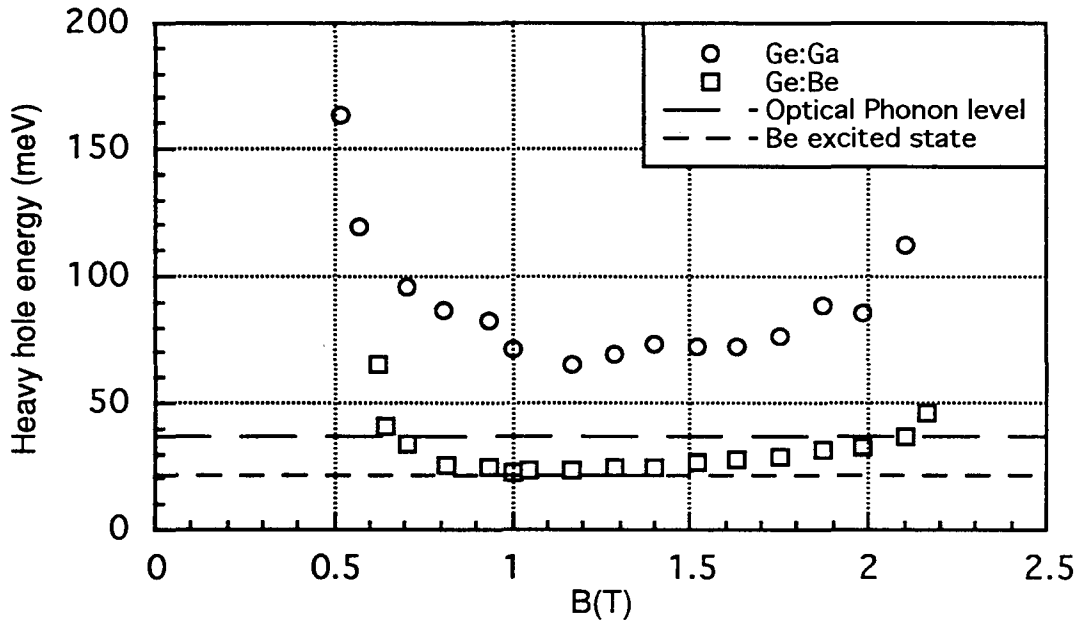

Figure 5-3: Computed heavy hole energies at onset of lasing for Ge:Ga (D06) and Ge:Be (D09).

because population inversion in Ge:Be occurs through a different mechanism than in Ge:Ga, as described in section 5.1.

The minimum and maximum theoretical limits are plotted with the lasing region in figure 5-2. The limits are calculated from equation 1.1 (table 5-1) as in chapter 4. For inversion via optical phonon emission, E_{max} in equation 1.1 was set equal to 37 meV, and for inversion via neutral impurities it was set equal to 20 meV. Clearly the limits found by setting the left-hand side of the equation equal to 20 meV match the observed lasing region well. From this we can see that the proposed mechanism of population inversion by energy transfer to neutral impurities matches the experimental evidence.

Another view of this data is presented in figure 5-3, which shows the heavy hole energies at the onset of lasing calculated from the data in figure 5-1. Again we see that these energies are very different, and correspond to two different mechanisms of population inversion.

5.3 Effect of uniaxial stress

The effect of 300 bar uniaxial stress on the beryllium-doped laser D09 is shown in figure 5-4. The uniaxial stress decreases the region in E and B in which the laser operates, as in the Ge:Ga laser (figure 4-3). We can attribute these results to a change in the fields needed to reach the threshold energy for inversion, as we saw for the Ge:Ga laser. The heavy hole effective mass decreases with applied pressure, so the electric field necessary for the heavy holes to achieve inversion increases. In addition, at low [100] stress the G-line bound excited state energy of the Be acceptor increases. [30] Both of these effects raise the lower theoretical limit for lasing. Since the light hole mass does not change much upon application of uniaxial stress, the small increase in the upper limit stems only from the increase in energy of the Be bound excited state.

Knowing how the effective mass and bound excited state energies change with pressure, we can calculate new theoretical limits for lasing. Values for the change in m* from reference [25] and the change in G-line energy of Ge:Be from reference [30] were used to calculate the limits given in table 5-1. These are shown graphically along with the data in figure 5-5. The increase in the lower limit for lasing matches well with the change in the data, and is due mostly to the decrease in heavy hole effective mass. In addition, the slight increase in lasing at high electric fields matches well with the theory and can be attributed to the slight increase in the G-line bound excited state energy upon uniaxial stress. It is evident that our proposed theory of population inversion in Ge:Be lasers matches well with the data we observe.

Stress	Be "G" energy (meV) [30]	heavy hole m* [25]	light hole m*	minimum E/B ($kV\ cm^{-1}T^{-1}$)	maximum E/B ($kV\ cm^{-1}T^{-1}$)
0 bar	20.0	0.35 m_o	0.042 m_o	0.709	2.046
300 bar	20.6	0.28 m_o	0.042 m_o	0.804	2.077

Table 5-1: Effect of stress on variables in equation 1-1.

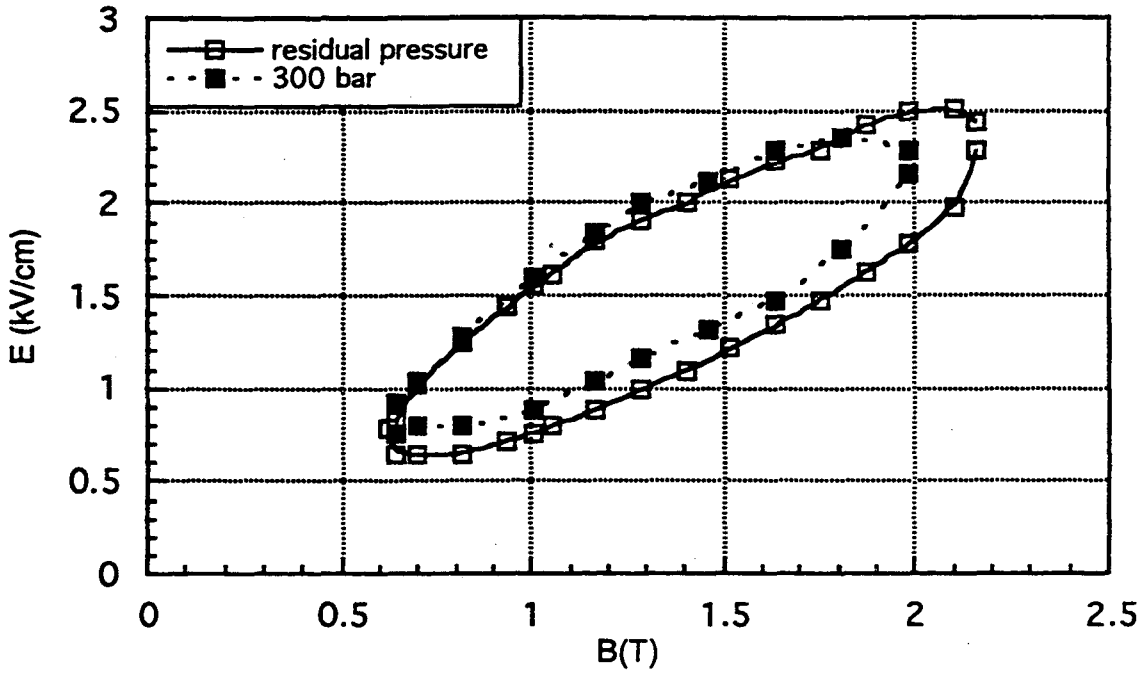

Figure 5-4: Conditions for lasing of crystal D09 with and without 300 bar [001] uniaxial stress.

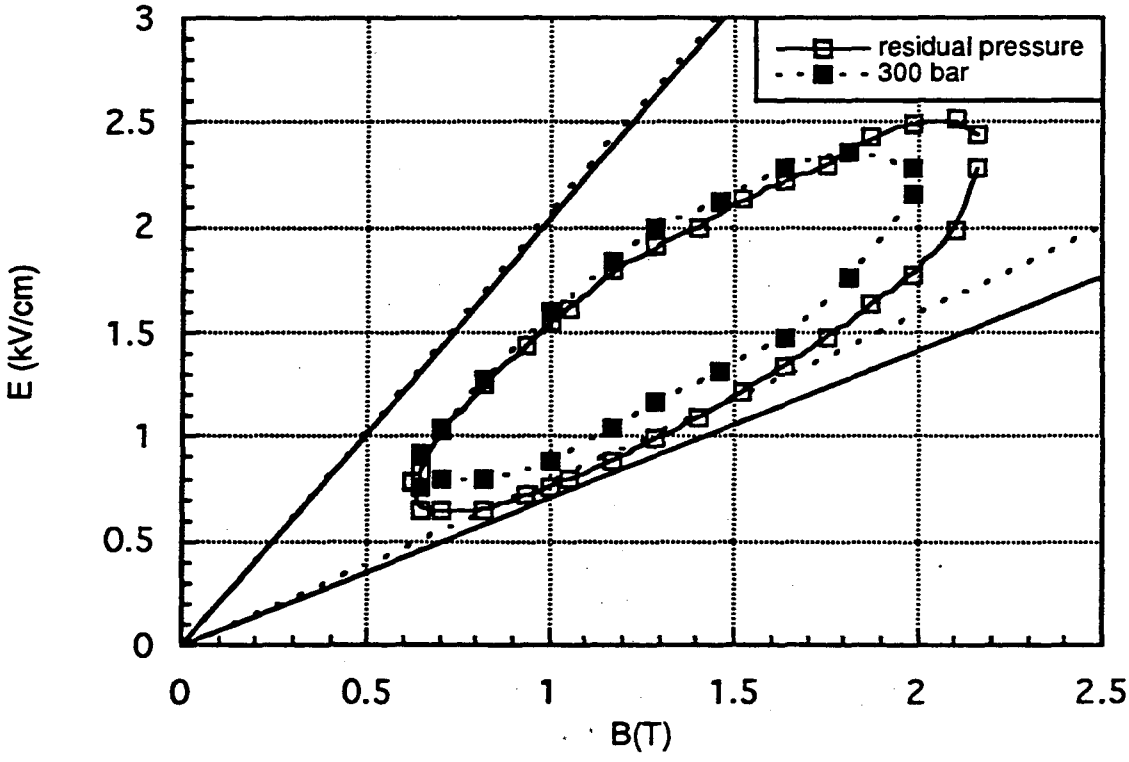

Figure 5-5: Conditions for lasing of D09 with theoretical minima and maxima calculated from equation 1-1.

6. Ge:Cu Lasers

6.1 Motivation for using Ge:Cu

Because of the success of Ge:Be lasers, hopes have been raised that multivalent-doped Ge FIR lasers will reach continuous-wave operation. Ideally, it will someday be possible to fabricate these lasers widely for FIR spectroscopy. However, beryllium-doped germanium is not a very common material because it historically has been used only for FIR detectors. Another material which is more easily available would be better.

Copper-doped germanium can be attained more easily than Ge:Be. It is fabricated using diffusion of copper into ultra-pure germanium, as discussed in section 3.1. Annealing temperatures range from 600-800 °C, which can be conveniently attained in a typical furnace tube. The solubility of copper in germanium at these temperatures ranges from 10^{14} to 10^{16} cm^{-3}, covering the concentrations needed for laser operation.

6.2 Lasing region - Ge:Cu

The magnitude of electric field and magnetic induction for Ge:Cu crystal D02 along with Ge:Ga crystal D06 are shown in figure 6-1. The theoretical limits shown are calculated assuming population inversion from optical phonon scattering (E_{max} = 37.2 meV). The Ge:Cu laser operates at lower electric fields than the Ge:Ga laser, but still within the theoretical limits. Since both lasers have the same crystal orientation, the hole effective masses during operation will be the same. However, in the Cu-doped laser the energy of the bound excited state corresponding to the G-line is 38.7 meV, which is greater than the light hole energies during laser operation. Thus the Cu-doped laser will not exhibit any "forbidden" or low-gain region around E/B = 1.2 kV cm^{-1} T^{-1}.

Lasing is not observed at high E/B in the copper-doped laser because the current increases and heats the laser too much. Since the neutral copper ionization level lies over four times deeper within the germanium bandgap than gallium, not all of the copper

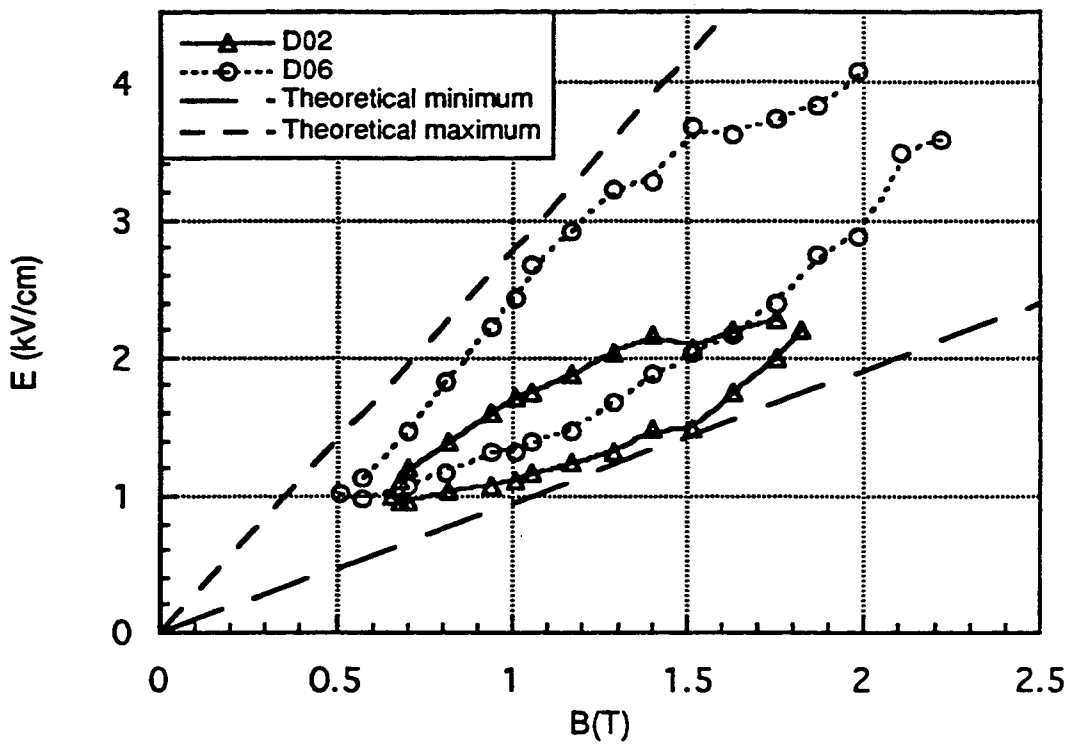

Figure 6-1: Conditions of electric field and magnetic induction for lasing in Ge:Cu laser D02 and Ge:Ga laser D06. Theoretical minimum and maximum are calculated based on inversion via optical phonon emission.

acceptors become ionized when the electric field is applied. In fact, the Ge:Cu laser must be more highly doped than the Ge:Ga laser to achieve the same hole current [15]. In the gallium-doped lasers, nearly all of the acceptors are ionized to generate the hole current, and the current does not change much as the electric field increases. However, only a fraction of acceptors are ionized when electric fields in the range of 1-5 kV/cm are applied to copper-doped germanium lasers. This fraction increases as the electric field increases, generating a larger current which in turn heats the laser faster.

6.3 Effect of uniaxial stress

6.3.1 Results

Because the energy of the Ge:Cu G-line lies so close to the optical phonon energy, it is not possible to determine whether the population inversion occurs like the

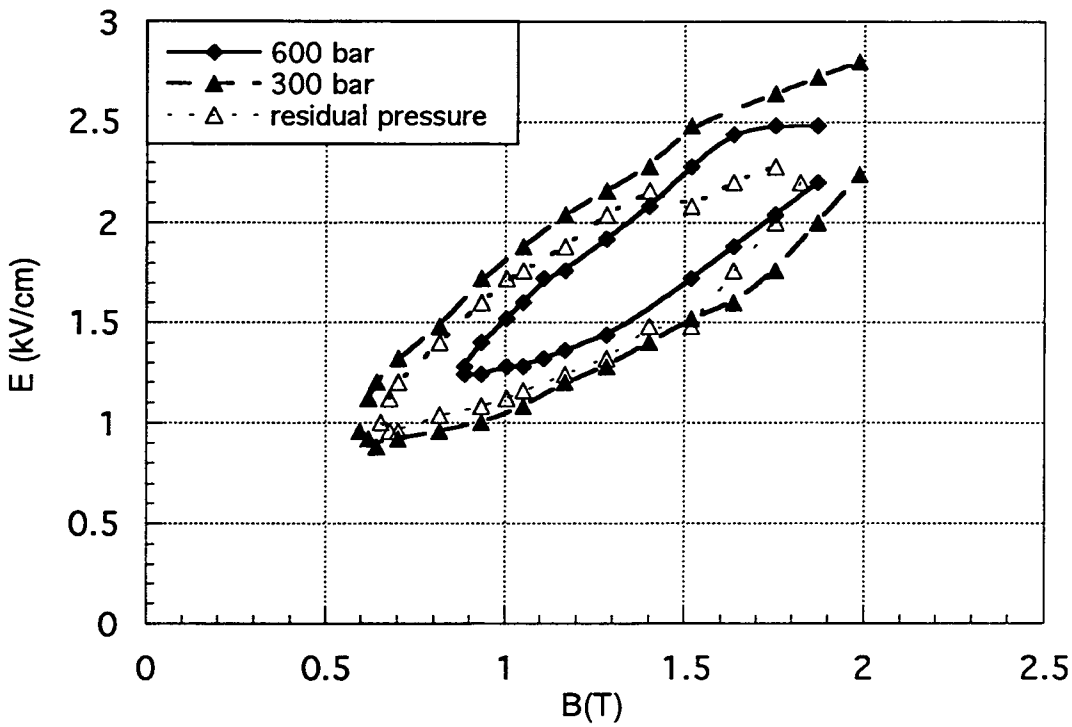

Figure 6-2: Conditions for lasing in Ge:Cu laser D02 at zero, 300, and 600 bar stress applied in the [001] direction.

mechanism for the Ge:Ga laser (phonon emission) or the Ge:Be laser (energy transfer to neutral acceptors). However, the energy of the excited state decreases upon the application of uniaxial stress [29], so pressure experiments can provide insight into the mechanism of population inversion in these lasers.

The E and B conditions for which lasing is seen in Ge:Cu crystal D02 are displayed in figure 6-2. Uniaxial stress of 300 bar in the [001] direction increases the region of lasing, *unlike the results for the beryllium and gallium-doped lasers*. Increasing the stress further to 600 bar decreases the region of lasing as was observed in the other two lasers.

6.3.2 Theoretical calculations

As in chapters 4 and 5, we can calculate new theoretical limits as a function of stress with data on the effective masses [25] and excited state energies [29]. Since we do not know whether the inversion is caused by optical phonon emission or energy transfer

to neutral acceptors, we must calculate the limits for both cases. The results are given in figures 6-3 and 6-4.

Figure 6-3 shows the calculated minimum E/B ratio for inversion via the two mechanisms. The limits are very close, and get even closer upon increasing pressure. Since the pressure in the crystal is not completely uniform due to the Hall field, these lines can be assumed to broaden (have error bars) at stress not equal to zero. With broadening, the lines will essentially coincide at all stresses larger than zero. If the energy needed for a heavy hole to transfer into the light hole band is the same, the hole can enter the light hole band via both mechanisms and the probability of the event occurring will increase.

Figure 6-4 shows the maximum E/B ratio for inversion via optical phonon emission and energy transfer to a neutral acceptor. The limit for inversion via optical

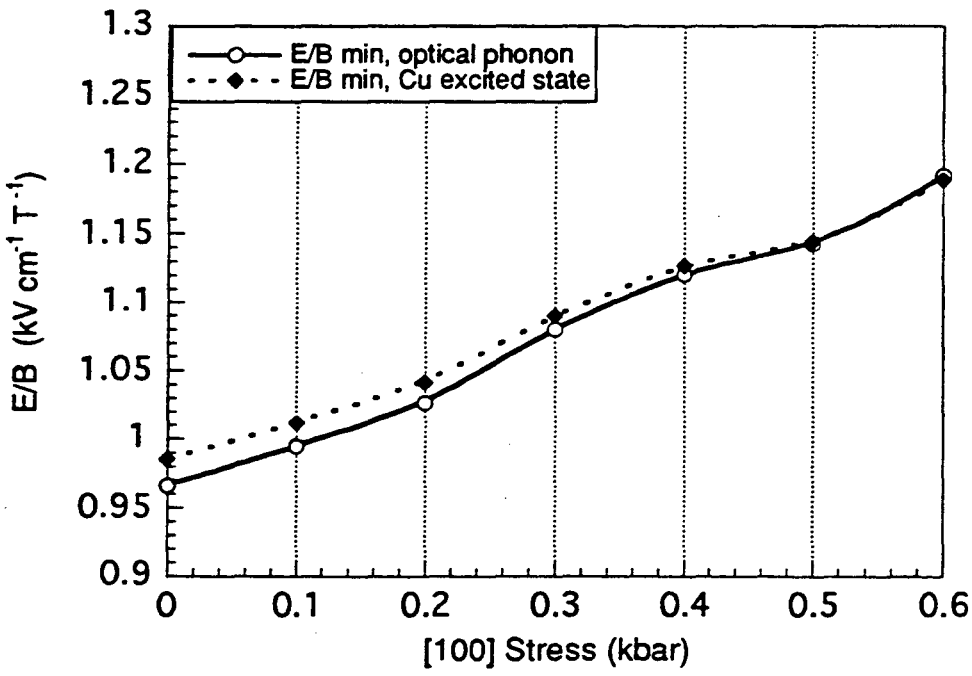

Figure 6-3: Calculated minimum E/B ratio necessary for population inversion as a function of [100] stress for two mechanisms: optical phonon emission and transfer of energy to a neutral copper acceptor.

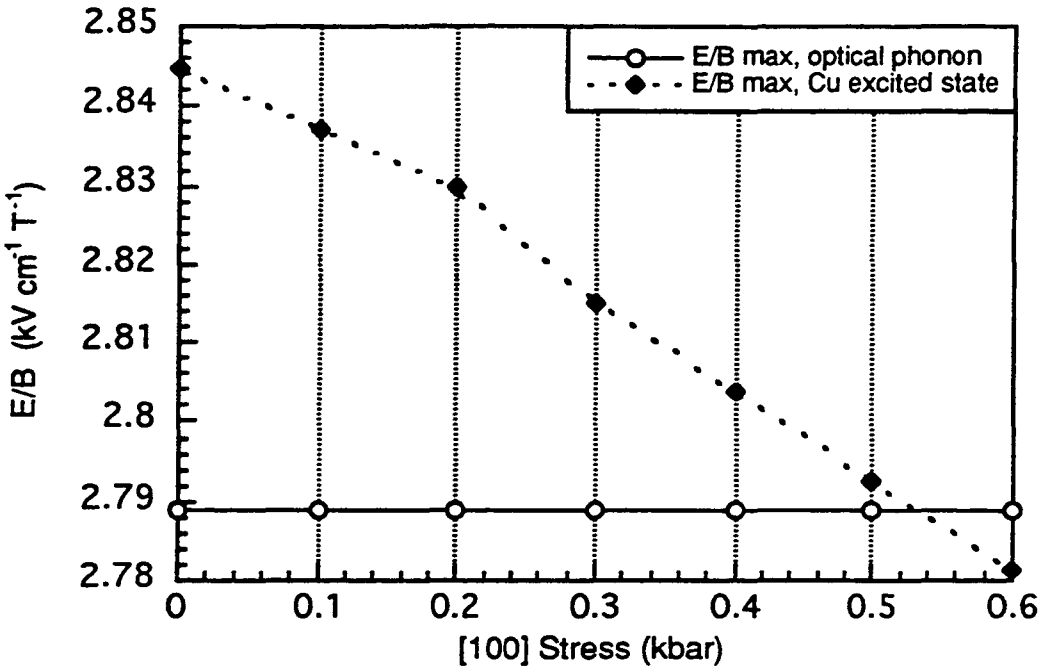

Figure 6-4: Calculated maximum E/B ratio necessary for population inversion to as a function of [100] stress for two mechanisms: optical phonon emission and transfer of energy to a neutral copper acceptor.

phonons (open circles) is invariant under uniaxial stress since both the light hole mass and the optical phonon energy are assumed to be insensitive to pressure. The decrease in the limit based on neutral acceptors (filled diamonds) is based on the decrease in bound excited state energy with pressure. The limits cross at a pressure of about 500 bar. Since the spread in the two maximum limits is relatively large at low pressures, we can conclude that at lower pressures the inversion will be destroyed by light holes emitting optical phonons. At higher pressures the inversion is destroyed through transfer of light hole energy to neutral Cu acceptors, since this requires a lower energy.

6.3.4 Explanation of results with theoretical calculations

The increase in the region of lasing with 300 bar uniaxial stress can be attributed to two factors: a) the limits do not decrease very much in the Ge:Cu laser under small

stress and b) the population inversion increases greatly when two mechanisms are available for transfer of holes into the light hole band. At higher pressures the minimum limit for lasing significantly increases. This decreases the lasing at low E/B as shown in figure 6-5. This figure shows the conditions for lasing of D02 at 300 and 600 bar along with the theoretical minimum limits at 0, 300, and 600 bar from figure 6-3. The data do follow the trend of the theory, however the theory predicts a higher threshold E/B than the data show. This can be explained with the poor pressure distribution shown in figure 3-2: if holes in some part of the laser crystal experience a lower pressure, they will invert at a lower E/B ratio.

The theoretical maximum limit for inversion does not decrease very much in figure 6-4, however, we observe a significant decrease in the maximum E/B ratio from the 300 to the 600 bar data. This is because the maximum E/B ratio in laser D02 is determined by crystal heating and not by the inversion limit as described in section 6.2. The heavy hole energy at a certain E/B ratio will increase under stress because the mass will decrease. This means the crystal will heat faster with increased stress at the same E/B, and the maximum E/B under stress will decrease.

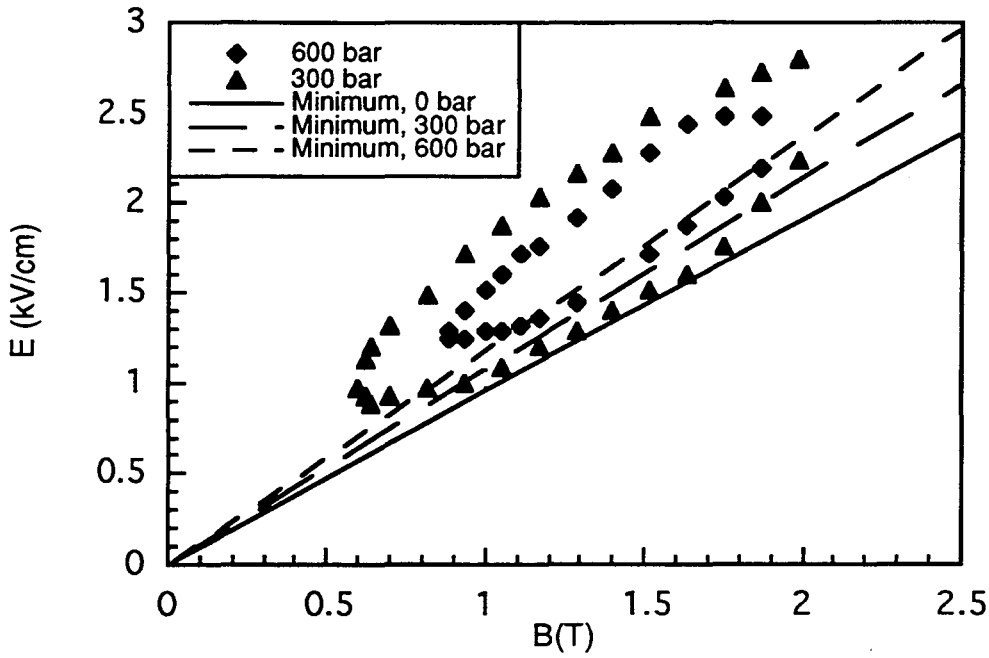

Figure 6-5: Conditions for lasing of D02 at 300 and 600 bar [001] stress, along with calculated minimum E/B ratio necessary for lasing at 0, 300, and 600 bar.

7. Conclusions

7.1 Summary

The effects of stress on germanium lasers doped with single, double, and triple acceptors have been investigated. The results can be explained quantitatively with theoretical calculations and can be attributed to specific changes in the energy levels of acceptors in germanium under stress.

In contrast to previous measurements, gallium-doped Ge crystals show a decrease in lasing upon uniaxial stress. The decrease seen here is attributed to the decrease in heavy hole effective mass upon application of uniaxial stress, which results in a decreased population inversion. The discrepancy between this work and previous studies can be explained with the low compensation level of the material used here. Because the amount of ionized impurity scattering in low-compensated germanium lasers is small to begin with, the reduction in scattering with uniaxial stress does not play a significant role in changing the laser operation.

Beryllium-doped germanium lasers operate based on a different mechanism of population inversion. In this material it is proposed that holes can transfer between bands by giving their energy to a neutral beryllium atom, raising the hole from the ground to a bound excited state. The free hole will then return to zero energy with some probability of entering the other band. The minimum and maximum E/B ratios for lasing change with uniaxial stress because of the change in effective mass and bound excited state energy. These limits have been calculated for the case of 300 bar [100] stress, and match very well with the observed data. This adds further credence to the proposed mechanism for population inversion in this material.

In contrast to Be and Ga-doped lasers, copper-doped lasers under uniaxial stress show an increase in the range of E and B where lasing is seen. To understand this change the theoretical limits for population inversion based on both the optical phonon mechanism and the neutral acceptor mechanism have been calculated. The data are

described by population inversion via optical phonons at zero pressure. However, both mechanisms most likely occur when the slightly higher, non-uniform pressures of 300 bar are applied, leading to an increase in population inversion and lasing. Upon further increasing the pressure to 600 bar, the limits for population inversion decrease and a decrease in the lasing is seen.

Since the dramatic increase in lasing at low fields expected with the application of uniaxial stress was not observed in these low-compensation, "high-quality" germanium crystals, it is unlikely that stressing hole inversion lasers will significantly help in the effort to achieve continuous-wave devices. However, this work has provided insight into the mechanisms of population inversion in multivalent acceptor-doped lasers, which are not yet fully understood.

7.2 Future Work

Further investigation into the deleterious effects of compensation would be interesting. This would provide valuable information as to the relative importance of ionized impurity scattering and acoustic phonon emission as non-radiative mechanisms for light holes to re-enter the heavy hole band. However, it is likely that this will lead to the conclusion that the lowest compensation level possible is the best and will not help in our efforts to achieve continuous-wave operation.

To progress towards continuous-wave operation, further miniaturization and better optical confinement is needed. This will increase the gain and decrease the current at the same time. Better optical confinement can be achieved by using gold mirrors sputtered on silicon. This should allow further miniaturization, since the minimum size necessary for lasing is now limited by the optical gain realized in a small laser crystal.

Further work could also be focused on increasing the cooling from these lasers. One design for achieving better cooling is to form a laser with a small "active" doped area adjacent to a large undoped area providing the cooling. These lasers could be fabricated

by diffusion of a thin Cu film from the surface, or with growth of Be-doped germanium by liquid phase epitaxy onto an ultra-pure germanium substrate. Hopefully with these improvements in cooling, miniaturization, and optical gain, we will be able to achieve a solid-state, continuous-wave, tunable, far-infrared laser.

Appendix I: Streaming motion

I.1 Hole motion in a large electric field

Under large electric fields and/or at low temperatures, carriers in a semiconductor will become "hot", having a drift velocity exceeding their thermal velocity. Under these conditions Ohm's law does not apply, and the current saturates with increasing electric field. At low electron or hole concentrations, the probability of interaction between carriers is very low. This means the mean free time τ for a carrier between inelastic scattering events depends only on the probability of emitting a phonon or interacting with an ionized impurity. In an electric field, a carrier will accelerate from zero drift velocity for time τ (on average) until it scatters and loses energy. It will then accelerate again just as before.

In *p*-Ge the probability of emitting an optical phonon becomes large when the

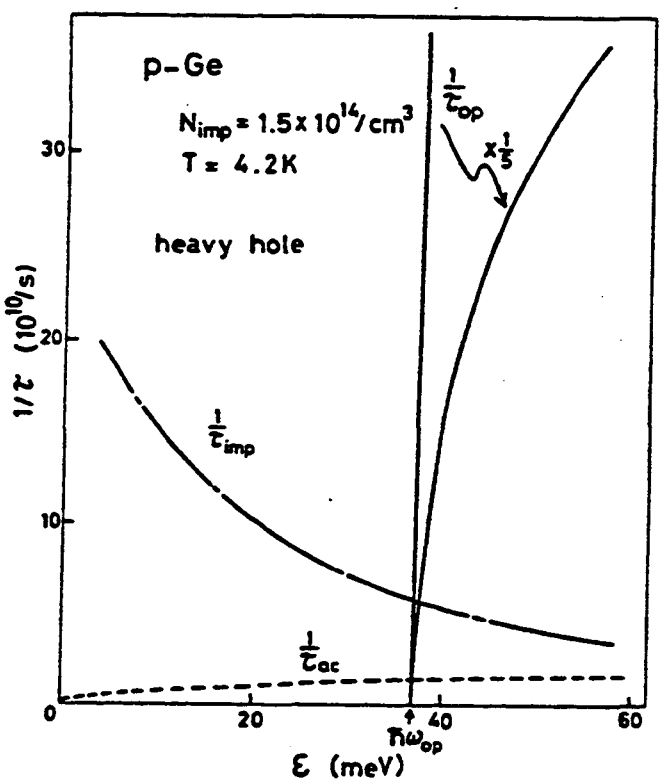

Figure I-1: Probability of scattering for heavy holes in germanium at 4.2 K as a function of heavy hole energy. Scattering is shown from ionized impurities (dash-dot line), acoustic phonons (dashed line), and optical phonons (solid line). (Courtesy Ref. [34])

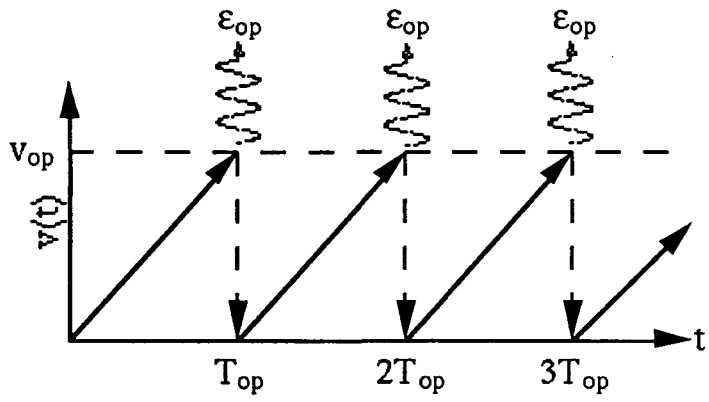

Figure I-2: Schematic drawing of "streaming motion".

holes have energy above 37 meV (Figure I.1 [34]). Because of this it is likely that carriers will increase their

velocity linearly until it reaches a critical value at:

$$1/2\ m^* v_{op}^2 = \mathcal{E}_{op} = 37.2\ \text{meV}. \qquad (I.1)$$

This occurs at time $t = \tau_{op}$, where

$$\tau_{op} = (2\ m^* \mathcal{E}_{op})^{1/2}(e\ E)^{-1} \qquad (I.2)$$

At this time, the hole will immediately emit an optical phonon and return to zero energy. If the probability of the hole emitting an optical phonon is much greater than the probability of scattering with an ionized impurity or emitting an acoustic phonon, the carriers will always reach the optical phonon energy and emit an optical phonon without exceeding it.(Figure I-2) This process is termed "streaming motion".[21] This condition is met when the mean free time dominated by acoustic phonon emission and ionized impurity scattering is longer than the mean free time from optical phonon emission, or

$$\tau_{op} < (\tau_{II}^{-1} + \tau_{AP}^{-1})^{-1} \qquad (I.3)$$

where τ_{II} is the average mean free time for scattering off of an ionized impurity and τ_{AP} is the average mean free time for emitting an acoustical phonon.

Combining equations (I.2) and (I.3) produces a lower limit for the electric field necessary for streaming motion. If the probability of ionized impurity scattering decreases, τ_{II} increases, the maximum τ_{op} for streaming motion will increase, and the

electric field necessary for streaming motion decreases. This is the explanation Komiyama and Kuroda use in their paper [10] to describe the decrease of lasing at lower electric fields upon application of uniaxial stress.

I.2 Hole motion in crossed electric and magnetic fields

Under the influence of both electric and magnetic fields, a hole will feel a Lorentz force equal to

$$\mathbf{F} = e(\mathbf{E} + \mathbf{v} \times \mathbf{B}) \tag{I.4}$$

which will cause the hole to follow a cycloidal trajectory as long as no scattering occurs. If the E and B fields are perpendicular, and we point them along the x and z axes, respectively, the components of force the hole feels will be:

$$\begin{aligned} F_x &= e\,E + e\,v_y\,B \\ F_y &= -e\,v_x\,B \\ F_z &= 0. \end{aligned} \tag{I.5}$$

Since $\mathbf{F} = m\,\mathbf{v}'$, we can set up the differential equations:

$$\begin{aligned} m^*\,v_x' &= e\,E + e\,v_y\,B \\ m^*\,v_y' &= -e\,v_x\,B \end{aligned} \tag{I.6}$$

In order to solve this system of differential equations, it will be easier to have only one equation. If we define a new variable

$$v = v_x + i\,v_y \tag{I.7}$$

we can add these two equations to get

$$m^*\,v' = e\,(E - i\,B\,v) \tag{I.8}$$

and use the trial solution

$$v = v_0 \exp\{i\omega t\} - (i\,E/B) \tag{I.9}$$

we find that this solution works when

$$\omega = e\,B/m^*. \tag{I.10}$$

Now, our trick of adding $v_x + i\,v_y$ is useful because we can extract out v_x and v_y by taking the real and imaginary parts of our solution v:

$$v_x = \mathrm{Re}\{V\} = v_0 \cos(\omega t)$$

$$v_y = \mathrm{Im}\{V\} = -v_o \sin(\omega t) - E/B \qquad (I.11)$$

and now we know the position in "velocity-space" that the hole will be at any time. Let us assume that at time t=0 the hole had no initial velocity, so $v_o = E/B$. The velocity of a hole at any subsequent time will be a point on the circle shown in Figure I-3. The magnitude of the hole velocity $|v|$ will be given by:

$$|v|^2 = v_x^2 + v_y^2 = 2v_o^2 (1 + \sin(\omega t)). \qquad (I.12)$$

Equation I.12 is plotted in Figure I-4. From this figure we see that $|v|^2$ oscillates and has a maximum at $4v_o^2$. Since the maximum hole energy is $1/2\ m^* |v|^2$ we obtain a maximum heavy hole energy of

$$E_{max} = 2\ m^* (E/B)^2 \qquad (1.1)$$

and we see that we have derived equation 1.1.

We achieve streaming motion when the maximum hole energy exceeds the optical phonon energy. This can be seen in Figure I-5. At a low E/B ratio, the maximum velocity is not large enough to cross the line denoting v_{op} in velocity space. This means that streaming motion is not observed. As E/B is increased, the circle that it follows in v-space will grow and will cross the v_{op} line denoting the velocity needed to emit optical phonons. At all E/B such that the hole velocity circle crosses the v_{op} line streaming motion will occur. Population inversion in germanium lasers is achieved under E/B conditions where heavy holes are in streaming motion and light holes are not.

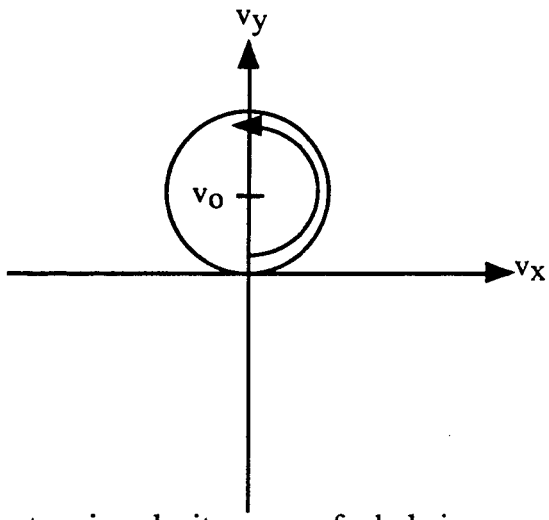

Figure I-3: Trajectory in velocity-space of a hole in crossed electric and magnetic fields.

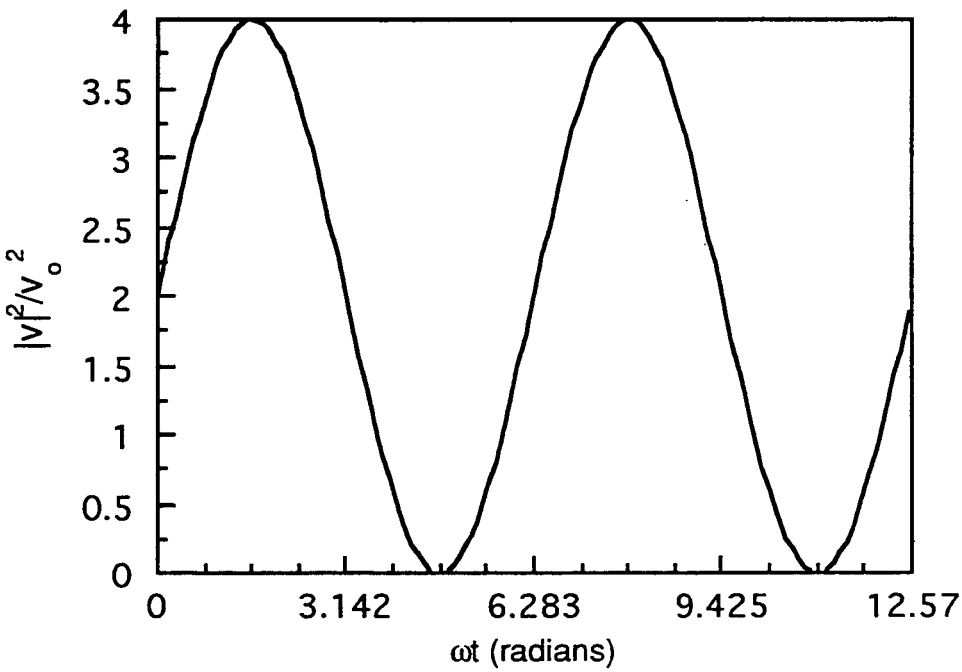

Figure I-4: Velocity squared of the hole shown in Figure I-3 as a function of time.

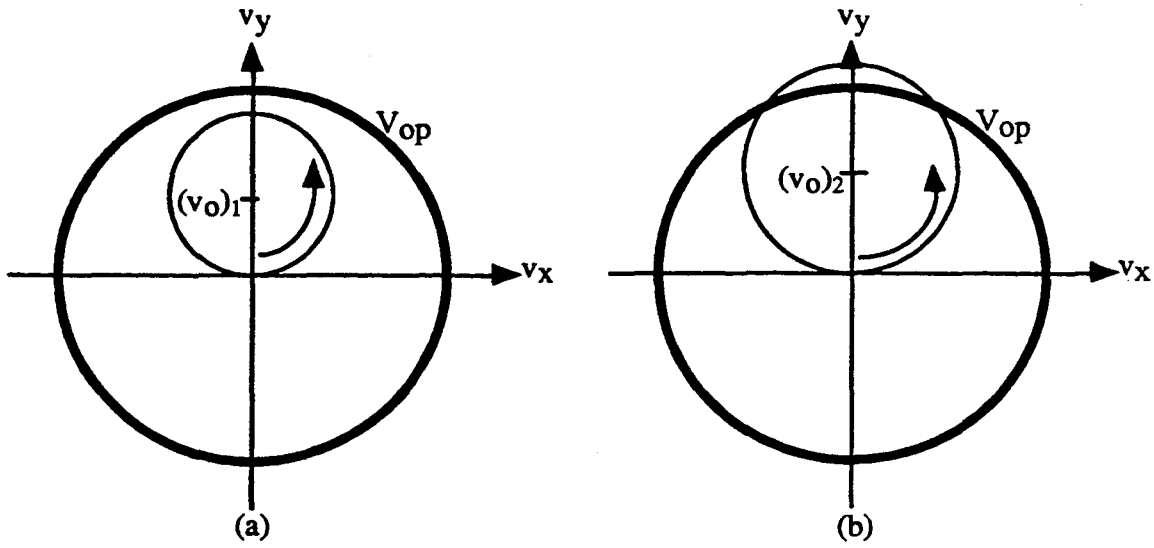

Figure I-5: Trajectories of a hole in velocity-space for two different values of E/B. (a): $2(v_o)_1 < v_{op}$; no streaming motion is observed and holes do not inelastically scatter. (b): $2(v_o)_1 > v_{op}$; streaming motion is observed and holes emit optical phonons.

Appendix II: Pressure rig

As described in section 3.5, a sample holder had to be designed which would let us apply 500 bar stress and 2 kV bias to the laser crystals while at 4.2 Kelvin inside a 1" bore superconducting magnet. For several reasons it was desirable to have the pressure variable from the outside of the cryostat. To effectively check the change in laser intensity as a function of pressure, it is necessary to increase the pressure continuously during a measurement. Heating the laser crystal up to room temperature to change pressure causes condensation to form on the crystal which can leave residue on the crystal surfaces which can increase optical losses and cause electrical shorts. In addition, several liters of helium are evaporated every time the holder at room temperature is placed into the liquid helium, so money is saved by removing the laser a minimum number of times.

The stringent requirements of electrical isolation, pressure, and tight tolerances restricted the design of the pressure rig severely. The final design consisted of:

(1) a sample holder to keep the laser inside the magnet

(2) an alignment block to hold the laser at right angles to the magnetic field

(3) a brass piston to supply both pressure and electrical contact

(4) a pivot bar to applied force to the brass piston

(5) a calibrated stainless steel spring to apply force to the pivot bar.

The design of the sample holder is shown in figure II-1. This piece is made entirely out of brass. It attaches to two concentric 1" and 0.5" diameter non-magnetic stainless steel pipes which serve to a) position the laser crystal inside the superconducting magnet, b) connect wires from the outside of the cryostat to the sample holder, and c) reflect the light from the laser crystal up towards the photoconductor, which is held within the innermost tube. A pivot bar, made from phosphor bronze, attaches to the 1/16" hole which is located 1.125" from the left side of the holder in figure II-1. At the other end of the pivot bar, a 6-32 brass screw with a hole drilled in the center is attached. One end of a long stainless steel wire is soldered into this screw, and the wire is fed around a

pulley located at the lower right corner of the holder as shown in figure II-1. The wire is then fed up the stainless steel tube to the outside of the cryostat. This wire is pulled from outside the cryostat to apply pressure to the laser.

The laser crystal is placed inside an alignment block and is centered 0.4" from the fulcrum of the pivot bar. Since the pivot bar is 4" long between the attached points, this gives a multiplication ratio of 10 to whatever force is applied externally on the stainless steel wire. The alignment block is shown in figure II-3. It was fabricated either from BN or from Lucite. The Lucite was easier to machine and more resistant to cracking than the BN. However, it also had a significant difference in thermal expansion than the brass piston it contained and therefore did not allow pressure to be varied at 4 Kelvin. The crystal is aligned by the 3 mm wide groove in the base of the block. This is centered with the 0.19" diameter hole which keeps the brass piston aligned. The tolerances on the piston and hole are tight to keep the applied pressure uniform. Kapton and mica are placed between the piston and the pivot bar for electrical isolation.

The wire attached to the pivot bar is fed up the stainless steel light pipes and outside of the cryostat. Here it is passed through a spring (figure II-4), which is held in a cavity which can be expanded or shrunk by twisting a threaded disc around the spring cavity as shown in the diagram. This spring container was borrowed from a stress rig built by A. Kazanskii *et al* [35] for uniaxial stress FIR spectroscopy. The wire is fixed at the end of a piston which presses on the spring. By changing the size of the spring cavity, the spring is compressed and puts a force on the piston and the wire. The piston has a ruler on it to measure the compression of the spring. Since the spring constant is known through calibration with weights, the force on the wire can be obtained.

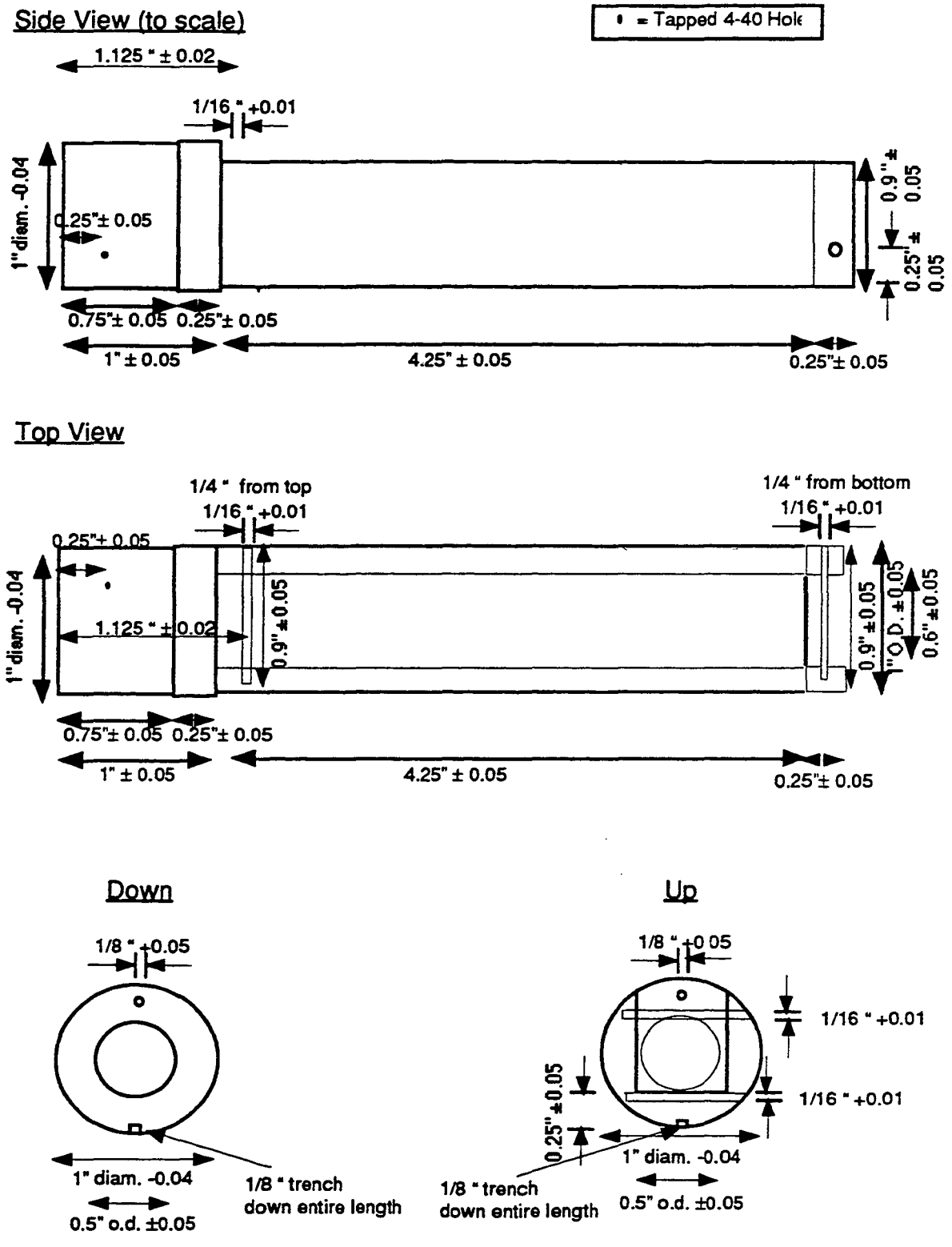

Figure II-1: Diagram of brass sample holder.

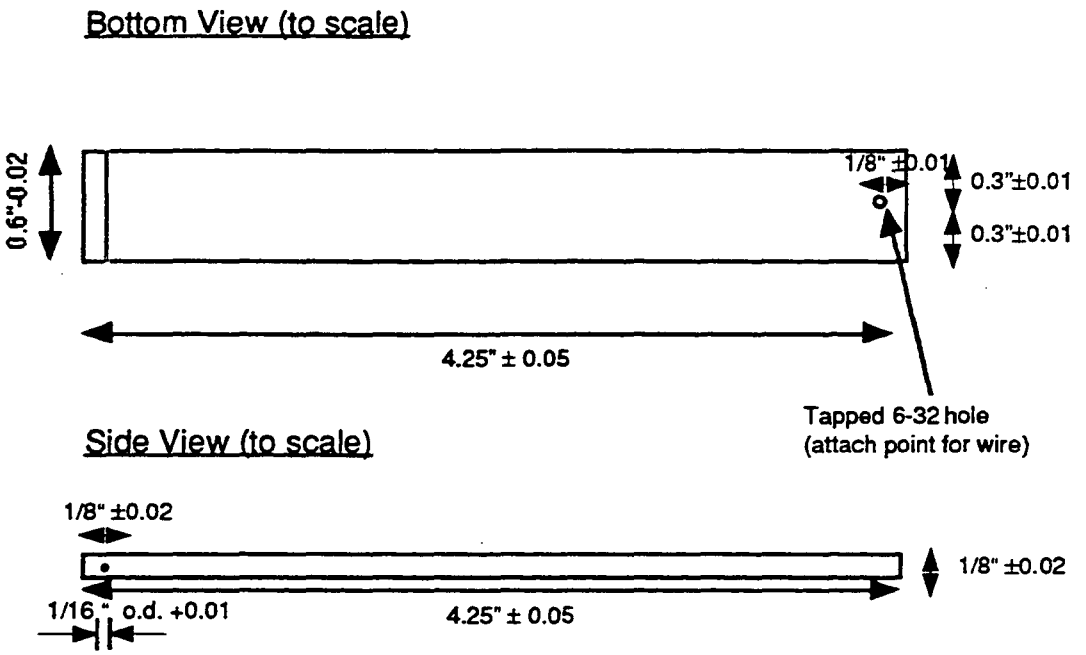

Figure II-2: Phosphor bronze pivot bar.

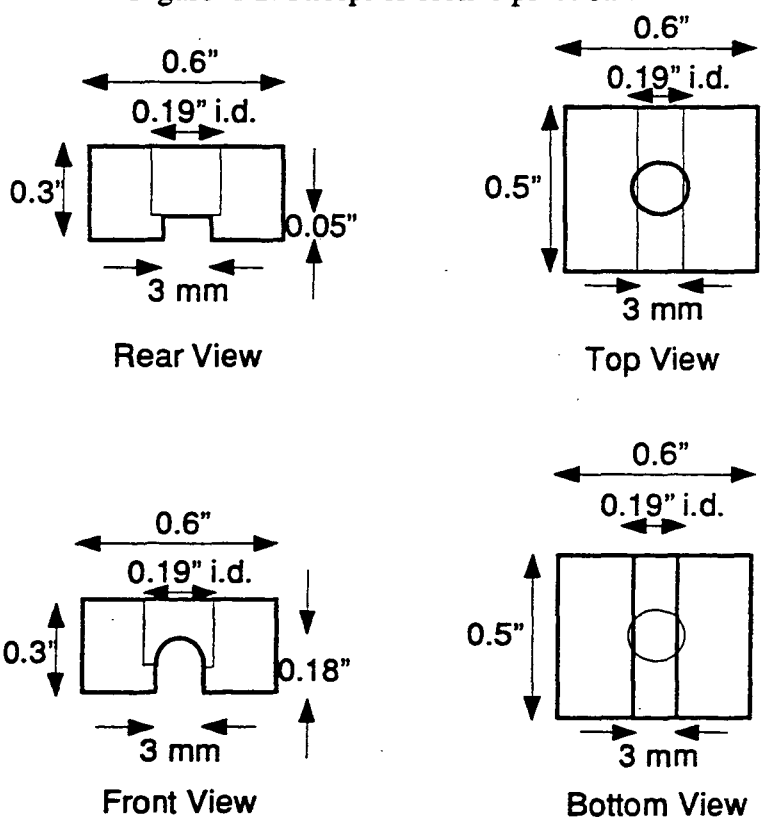

Figure II-3: Four views of the BN or Lucite alignment block. Thicker lines mean edges are visible from this view; thinner lines are on the opposing side of the block.

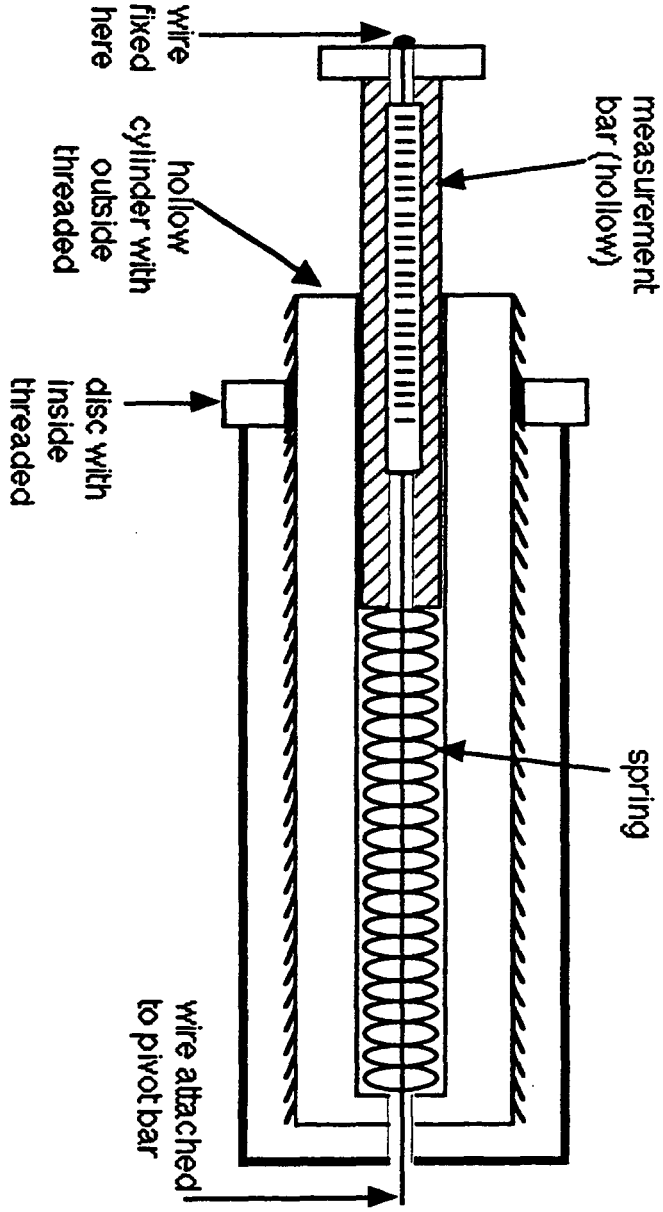

Figure II-4: Cross-sectional view of device used to apply force to stainless steel wire connected to the pivot bar.

References

1. Elizabeth Corcoran and Glenn Zorpette, "Diminishing Dimensions,":*Scientific American* Special Issue October 1997, pp. 25-33.

2. G. Dresselhaus, A. F. Kip, and C. Kittel, "Cyclotron resonance of electrons and holes in silicon and germanium crystals," *Physical Review* **98**(2):368-384, 1955.

3. R. N. Dexter, H. J. Zeiger, and B. Lax, "Cyclotron resonance experiments in silicon and germanium," *Physical Review* **104**(3):637-644, 1956.

4. H. Maeda and T. Kurosawa, "Hot electron population inversion in crossed electric and magnetic fields," *Journal of the Physical Society of Japan*, **33**:562, 1972.

5. A. A. Andronov, V. A. Kozlov, L. S. Mazov, and V. N. Shastin, "Amplifications of far-infrared radiation in germanium during the population inversion of 'hot' holes," JETP Letters **30**(9):551-555, 1979.

6. S. Komiyama, "Far-infrared emission from population-inverted hot-carrier system in p-Ge," *Physical Review Letters* **48**(4):271-274, 1982.

7. A. A. Andronov, I. V. Zverev, V. A. Kozlov, Y. N. Nozdrin, S. A. Pavlov, and V. N. Shastin, "Stimulated emission in the long-wavelength IR region from hot holes in Ge in crossed electric and magnetic fields," *JETP Letters* **40**(2):804-807, 1984.

8. Yu. L. Ivanov and Yu. B. Vasil'ev, "Submillimeter emission from hot holes in germanium in a transverse magnetic field," *Soviet Technical Physics Letters* **9**(5):264-265, 1983.

9. Yu. A. Mityagin, V. N. Murzin, S. A. Stoklitskii, and I. E. Trofimov, "Anticrossing of Landau levels and stimulated emission of hot holes in germanium in the cyclotron-transition region," *JETP Letters* **46**:144-147, 1987.

10. S. Komiyama and S. Kuroda, "Remarkable effects of uniaxial stress on the far-infrared laser emission in *p*-type Ge," *Physical Review B* **38**(2):1274-1280, 1988.

11. C. Kremser, W. Heiss, K. Unterrainer, E. Gornik, E. E. Haller, W. L. Hansen, "Stimulated emission from *p*-Ge due to transitions between light-hole Landau levels and excited states of shallow impurities,". *Applied Physics Letters* **60**(15):1785-7, 1992.

12. W. Heiss, K. Unterrainer, E. Gornik, W. L. Hansen, E. E. Haller, "Influence of impurity absorption on Ge hot-hole laser spectra," *Semiconductor Science and Technology* **9**:638-640, 1994.

13. E. Bründermann, A. M. Lindhart, L. Reichertz, H. P. Röser, O. D. Dubon, W. L. Hansen, G. Sirmain, and E. E. Haller, "Double acceptor doped Ge: A new medium for inter-valence band lasers," *Applied Physics Letters* **68**(22):3075-3077, 1996.

14. L. A. Reichertz, O. D. Dubon, G. Sirmain, E. Bründermann, W. L. Hansen, D. R. Chamberlin, A. M. Linhart, H. P. Röser, and E. E. Haller, "Stimulated far-infrared emission from combined cyclotron resonances in germanium," *Physical Review B* **56**(19):12069-12072, 1997.

15. G. Sirmain, L. A. Reichertz, O. D. Dubon, E. E. Haller, W. L. Hansen, E. Bründermann, A. M. Linhart, and H. P. Röser, "Stimulated far-infrared emission from copper-doped germanium crystals," *Applied Physics Letters* **70**(13):1659-1661, 1997.

16. V. N. Shastin, "Hot hole inter-sub-band transition p-Ge FIR laser," *Optical and Quantum Electronics* **23**:S111-131, 1991.

17. E. Bründermann, A. M. Linhart, H. P. Röser, O. D. Dubon, W. L. Hansen, and E. E. Haller, "Miniaturization of p-Ge lasers: Progress toward continuous wave operation," *Applied Physics Letters* **68**(10):1359-1361, 1996.

18. E. Bründermann, A. M. Linhart, H. P. Röser, O. D. Dubon, W. L. Hansen, and E. E. Haller, "Miniaturization of p-Ge lasers: Progress toward a tunable, continuous wave THz laser," presented at the 7th International Symposium on Space Terahertz Technology, March 12-14, 1996, University of Virginia, Charlottesville, VA.

19. D. R. Chamberlin, unpublished data.

20. O. D. Dubon, D. R. Chamberlin, W. L. Hansen, E. E. Haller, L. A. Reichertz, G. Sirmain, E. Bründermann, A. M. Linhart, and H. P. Röser, "Terahertz emission from *p*-type germanium lasers doped with novel acceptors," presented at the 8th International Symposium on Space Terahertz Technology, March 25-27, 1997, Harvard University, Cambridge, MA.

21. W. E. Pinson and R. Bray, "Experimental determination of the energy distribution functions and analysis of the energy-loss mechanisms of hot carriers in *p*-type germanium," *Physical Review* **136**(5A):A1449-1466, 1964.

22. K. W. Böer, Survey of Semiconductor Physics. Van Nostrand Reinhold, New York, 1990, chapters 32 and 33.

23. F. Szmulowicz, "Calculation of optical- and acoustic-phonon-limited conductivity and Hall mobilities for *p*-type silicon and germanium," *Physical Review B***28**(10):5943-5963, 1983.

24. G. E. Pikus and G. L. Bir, "Effect of deformation on the hole energy spectrum of germanium and silicon," *Soviet Physics - Solid State* **1**:1502-1517, 1960.

25. O. D. Dubon, Electronic processes in uniaxially stressed *p*-type germanium, PhD Thesis, U.C. Berkeley, 1996, unpublished, LBL report #38287.

26. J. C. Hensel and K. Suzuki, "Quantum resonances in the valence bands of germanium. II. Cyclotron resonances in uniaxially stressed germanium," *Physical Review B* **9**: 4219, 1974.

27. A. D. Martin, P. Fisher, C. A. Freeth, E. H. Salib, and P. E. Simmonds, "Deformation potential constants of gallium impurity in germanium," *Physics Letters* **99A**(8):391-395, 1983.

28. R. L. Jones and P. Fisher, "Spectroscopic study of the deformation-potential constants of group-III acceptors in germanium," *Physical Review B* **2**(6):2016-2029, 1970.

29. E. H. Salib, P. Fisher, and P. E. Simmonds, "Quantitative piezospectroscopy of

neutral copper in germanium," *Physical Review B* **32**(4):2424-2438, 1985.

30. J. W. Cross, C. R. LaBrec, S. Rodriguez, A. K. Ramdas, and E. E. Haller, "A piezospectroscopic study of Be double acceptors in Ge," *Physical Review B* **32**(12):7992-8001, 1985.

31. H. Bracht, N. A. Stolwijk, and H. Mehrer, "Diffusion and solubility of copper, silver, and gold in germanium, "*Physical Review B* **43**(18):14465-14477, 1991.

32. V. I. Gavrilenko and V. V. Nikonorov, "Remarkable effects of uniaxial stress on stimulated far-IR emission from hot holes in germanium in crossed electric and magnetic fields," *Optical and Quantum Electronics* **23**:S217-220, 1991.

33. V. I. Gavrilenko, N. G. Kalugin, Z. F. Krasil'nik, V. V. Nikonorov, A. V. Galyagin, and P. N. Tsereteli, "Inverted distribution of hot holes in uniaxially stressed germanium," *Semiconductor Science and Technology* **7**:B649-651, 1992.

34. S. Komiyama, "Streaming motion and population inversion of hot carriers in crossed electric and magnetic fields," *Advances in Physics* **31**(3):255-297, 1982.

35. A. G. Kazanskii, P. L. Richards, and E. E. Haller, "Far-infrared photoconductivity of uniaxially stressed germanium," *Applied Physics Letters* **31**(8):496-7, 1977.
A. G. Kazanskii, P. L. Richards, and E. E. Haller, "Photoionization of acceptors in uniaxially stressed germanium," *Solid State Communications* **24**(9):603-6, 1977.

Ernest Orlando Lawrence Berkeley National Laboratory
One Cyclotron Road | Berkeley, California 94720

Prepared for the U.S. Department of Energy under Contract No. DE-AC03-76SF00098